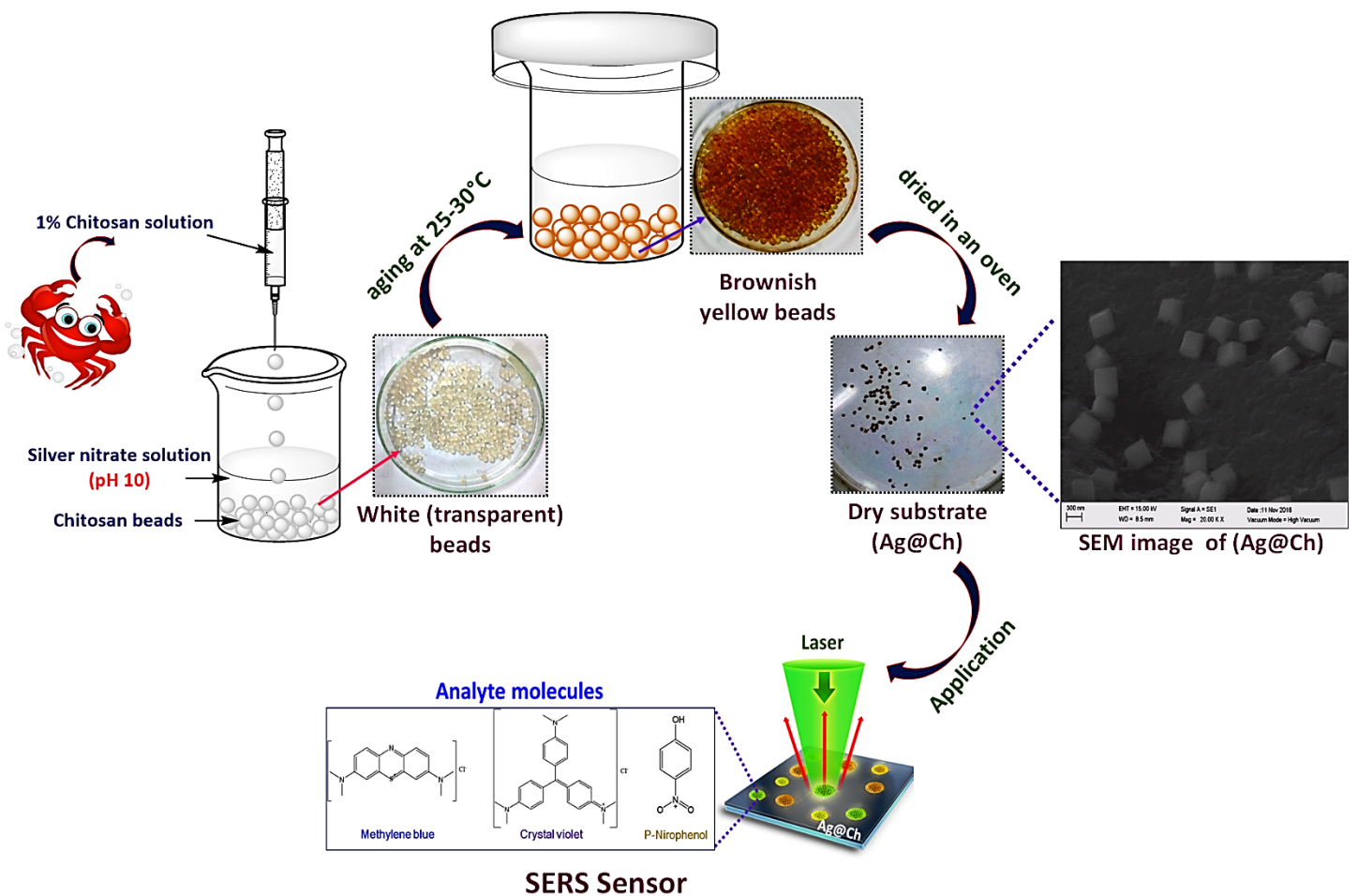


Chapter 2: Chitosan supported monolayer assembly of Silver Nanostructures as SERS substrates



2.1. Introduction

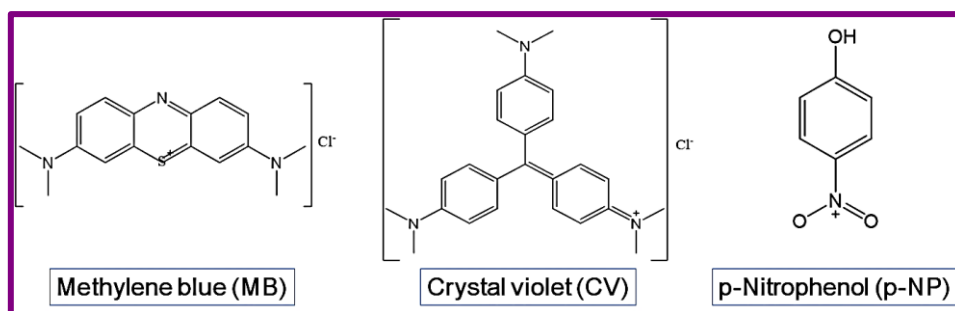
Surface-enhanced Raman scattering, is a commonly used attractive sensing technique with enhancement factors up to 10^8 or even higher, where the molecules are adsorbed onto corrugated or rough metal surfaces such as silver or gold nanoparticles. Ag is one of the best SERS substrates, its dielectric constant being close to the Frohlich frequency causes a strong surface plasmon absorption in the visible wavelength range (Saito et al., 2002). Solid SERS substrates are more stable, reproducible and very efficient as compared to the colloidal suspensions, and can be stored for long time without losing its SERS properties (K. Wang et al., 2019). The molecules of analyte are adsorbed between the nanoparticles (hot spot) or on the metal surface. Due to this close proximity, the surface plasmon resonance (SPR) in metal nanoparticle produces an amplified electromagnetic field that increases the intensity of Raman signals and helps to identify trace level analytes present in the sample.

The supports for the nanostructures play an important role for the nanoparticles to act as SERS substrate. The important supports are, metal oxides, graphene, silica and polymers (Tong et al., 2018). Chitosan is gaining interest as matrix material for immobilization of nanoparticles and nanostructures due to its ability to act as reducing agent, control and direct the particle growth as well as stabilize the particles, thus resulting in biogenic nanomaterials with new or improved properties (Nhung & Lee, 2014). Metal nanosystems supported by chitosan are efficient and biocompatible SERS substrate as they form hot-spots between interconnected nanoparticles which are responsible for increased local electromagnetic fields and in turn, enhancing Raman scattering of probe molecules in this region (Potara et al., 2012).

Recently research has been done to develop wrinkled metallic surfaces to increase the intensity of Raman signal (Duan et al., 2018). Maddipatla et al. developed a novel wrinkle-structured SERS substrate for the detection of cocaine. Gravure printing was used to deposit Ag NP ink on a stretchable, flexible thermoplastic polyurethane substrate to create the SERS substrate. (Maddipatla et al., 2019). A SERS substrate based on Ag NPs loaded chitosan foam was synthesized using citrate as reagent under microwave irradiation by Wang et al. and has been applied for the detection of Nile Blue A and Rhodamine 6G (C. Wang et al., 2019). Jung et al. have fabricated chitosan-Ag by using sodium borohydride as reductant, with rigorous stirring, followed by freeze drying at $-70\text{ }^{\circ}\text{C}$ and lyophilization for 24 h (Jung et al., 2013). Chitosan and AgNO_3 were mixed by Chevva et al. and kept for low power ultra-sonication till the appearance of violet color, confirming the formation of silver in the solution and used it for

detection of Rhodamine 6G (Chevva et al., 2017). Monitoring of catalytic reduction of 4-nitrophenol (p-NP) by SERS was done by M. Muniz-Miranda (Muniz-Miranda, 2014). He prepared Ag nanoparticles doped titania colloidal nanocomposite to monitor the catalytic reduction of p-Np under UV irradiation.

However, the fabrication techniques were expensive and sophisticated (He et al., 2017). Reusable, biodegradable chitosan-based silver nanostructures are easy to prepare with proven economic viability and can be stored or rapid SERS measurement could be acquired as the situation demands. This makes Ag@Ch substrate a promising platform for Raman analysis. In the present study an attempt was made to prepare wrinkled chitosan supported silver nanostructures (Ag@Ch) by self-assembly in order to avoid aggregation and improve the stability of Ag NPs as well as to avoid dissociation of Raman probe molecules. The potential of Ag@Ch as SERS substrates was investigated using Crystal Violet (CV), Methylene blue (MB) and p-Nitrophenol (p-NP) as model analyte probes as well as by monitoring the progress of catalytic reduction of p-Nitrophenol. In depth analysis of the mechanistic aspects has been attempted by DFT studies.



2.2. Materials and Methods

2.2.1. Materials

All chemicals were purchased as analytical grade from commercial suppliers and were used without further purification. Chitosan (from crab shells) was purchased from Sigma-Aldrich (75–85% deacetylated of mean molecular weight ~190,000–310,000 Da). The synthesized nanostructures (Ag@Ch) were first dried in oven at 120 °C and then used for further analysis.

2.2.2. Fabrication of chitosan supported silver nanocubes (Ag@Ch)

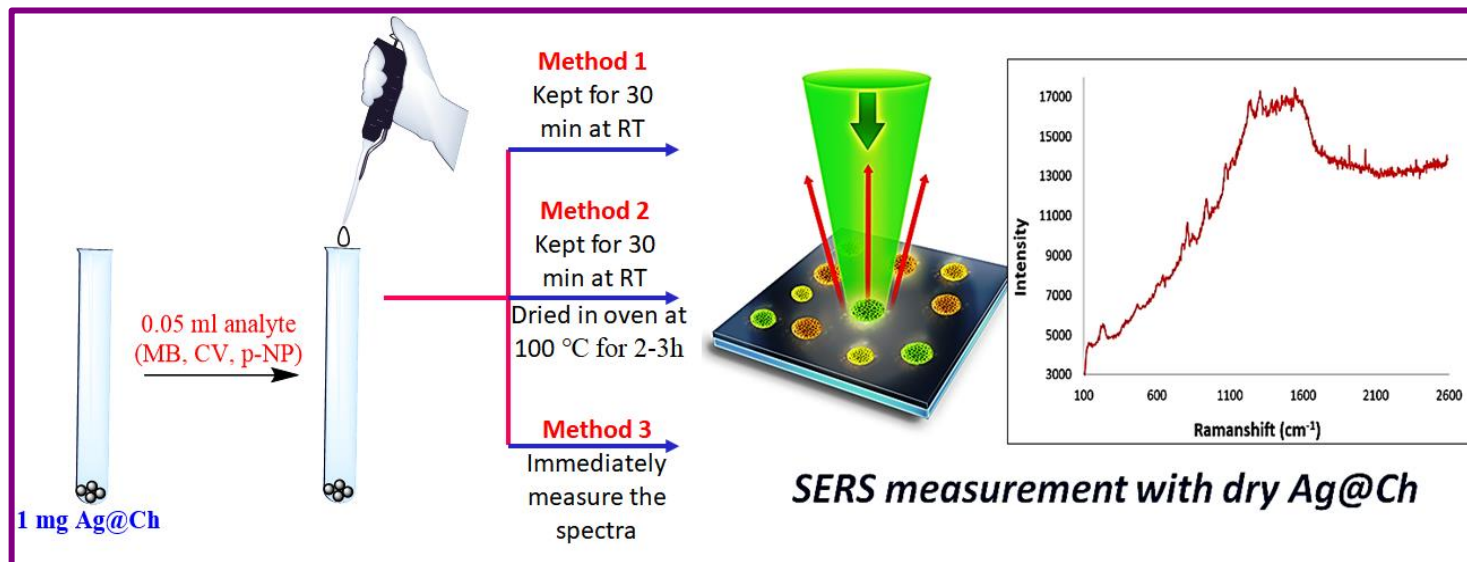
The chitosan supported silver nanostructures (Ag@Ch) were fabricated by first preparing 1% chitosan solution (0.1 g Chitosan in 10 mL 1% acetic acid solution). Further, 10 mL of 0.1 M

silver nitrate solution was prepared and adjusted to pH 10 using liquor ammonia. The chitosan solution was then added drop wise using syringe pump into AgNO_3 solution to form transparent beads and were kept for aging at 25-30°C. After 4 days the beads, turned yellowish brown in color indicating the assembly of silver nanoparticles on chitosan matrix. The beads were collected, washed 2-3 times with 50 mL of conductivity water to remove residual alkali and dried in an oven for 8-10 h at 120 °C resulting in the formation of brown colored silver nanoparticles on chitosan matrix(Kumara Swamy et al., 2015).

Silver nitrate in ammoniacal solution resulted in the formation of silver amine complex while chitosan is soluble in acetic acid due to its protonated amino groups. During dropwise addition of chitosan to ammoniacal solution, small chitosan beads were formed which slowly swelled as the solution neutralized with simultaneous assembly of silver ions, the diffusion of Ag^+ being restricted by the polymer network (Nate et al., 2018)

2.2.3. Preparation of SERS Substrates for sensing dyes and nitrophenol

Samples for SERS measurements were prepared in 3 ways by using the dried Ag@Ch nanostructures.



Scheme 2.1: Schematic diagram of SERS measurement by 3 methods

Method 1: Requisite amount (0.05 mL) of analyte solution (p-NP, MB, CV) was taken in a small vial. A known amount of Ag@Ch (i.e., 1 mg) was added to the solution and kept at room temperature (25-30°C) for 30 min and was used for SERS measurement.

Method 2: 1 mg of Ag@Ch was taken in a small test tube and 0.05 mL of analyte solution (p-NP, MB, CV) were added and kept at room temperature (25-30°C) for 30 min. These samples were kept for drying in oven at 100°C for 2-3 h and were further used for SERS measurement.

Method 3: 1 mg of Ag@Ch was kept on slide to which 0.05 mL of analyte solution (p-NP, MB, CV) was added and SERS spectra were recorded immediately.

2.2.4. Optimization of SERS measurement of dyes and nitrophenol

Method 1 was adapted for SERS measurement of dyes while method 3 was used for monitoring nitrophenol reduction process. Optimization of parameters were done by adapting Method1.

(A) Optimization of amount of Analyte

About 10 mg of Ag@Ch was taken into a small test tube and different amounts (0.01 mL to 0.05 mL) of 30 ppm of analyte under study was added and kept at room temperature (25-30°C) for 30 min and used for SERS measurement.

(B) Optimization of amount of SERS Substrate

Different amounts of Ag@Ch (0.5mg, 1mg, 5mg, 10mg) was taken into a small test tube followed by 0.05 mL of 30 ppm of analyte under study. The test tubes were kept at room temperature (25-30°C) for 30 min and were further used for SERS measurement.

Optimized amount of analyte and substrate were used for further studies.

2.2.5. Catalytic Reduction of p-NP: (monitored by Raman spectroscopy)

A 10 mL of 10 ppm p-NP and 1 mg of Ag@Ch were taken in a vial and the Raman spectra was recorded. After that 2 mg of sodium borohydride was added to reaction mixture and Raman spectra were recorded in the interval of 5 min to monitor the reduction process.

2.2.6. Characterization techniques and methods of analysis of synthesized SERS substrate (Ag@Ch)

For the morphological analysis of the prepared nanostructured samples, Scanning Electron Microscopy (SEM) of the samples was performed. Elemental composition of the catalyst was determined by Energy dispersive X-ray spectroscopy (EDS). The average particle size of the prepared Ag nanoparticles was determined by High resolution Transmission electron microscope (HRTEM). The structural characterization of the synthesized Ag@Ch was done

using powder X-ray diffraction (PXRD). TG-DTA was employed to analyze the population of surface functional groups on the basis of thermal stability. Fourier transform infrared (FTIR) analysis was applied to determine the functional groups. X-Ray Photoelectron Spectroscopy (XPS) was used to analyse the surface composition and oxidation states of silver nanoparticles as well as their modes of binding when loaded onto chitosan.

2.2.6.1. SEM-EDS

Scanning Electron Microscopy (SEM) images were taken using (SEM ZEISS EVO 18) instrument. A dried sample was placed on metal stub with adhesive. Elemental composition of the catalyst was determined by Energy dispersive X-ray spectroscopy (EDS) using a JSM 7600F spectrometer. The intensity of a peak in an EDS spectrum is directly proportional to the concentration of the corresponding element on the surface of the specimen.

2.2.6.2. FTIR analysis of Ag@Ch

FTIR analysis was carried out to identify the vibrational frequencies of the functional groups present in the prepared nanosystems. The spectra were collected using a BRUKER optics, IR spectrometer within the wave number range of 400-4000 cm^{-1} . Specimens of samples were first mixed with KBr and then ground in an agate mortar at an appropriate ratio of 1/100 for the preparation of the pellets. Resulting mixture was pressed under vacuum at 10 tons for 5 min. and were applied for recording spectra. The background obtained from the scan of pure KBr was automatically subtracted from the sample spectra in order to remove instrument and atmospheric contributions from the sample spectra.

2.2.6.3. Powder-XRD

X-ray diffraction is an effective and non-destructive technique for analysing the crystalline samples including nanoparticles. PXRD of the nanosystems was performed using Bruker D8 Focus Diffractometer with $\text{Cu K}\alpha$ radiation of wavelength 1.5406 Å at room temperature over a range of 10-80° 2 θ . and the XRD pattern was plotted and analysed by using Origin software.

2.2.6.4. TG-DTA analysis

Thermo gravimetric analysis (TGA) is an analytical method that analyses the weight change that takes place as a specimen is heated in order to assess a material's thermal stability and the percentage of volatile components. Thermo gravimetric analysis was done by TG-DTA-6300, INCARP EXSTAR 6000 instrument under nitrogen atmosphere. 5-10 mg of the sample was

weighed, taken in the sample pan and the temperature was raised from 30 to 750°C at a heating rate of 10 °C per minute. The mass of the sample pan was continuously recorded as a function of temperature.

2.2.6.5. HRTEM analysis

The morphology, particle size and composition of nanoparticles were characterized by using High resolution transmission electron microscopy (HRTEM) JEOL (JEM 2100F Model) instrument, operated at an accelerating voltage 200kV. Samples were taken in water and sonicated for 30 min and were placed on Cu coated TEM grid by drop casting method.

2.2.6.6. XPS Analysis

The Ag@Ch was analyzed by X-ray Photoelectron spectroscopy to determine the chemical states. X-ray photoelectron spectroscopy (XPS) analysis was carried out with VG Microtech multilab ESCA 3000 spectrometer. Background subtraction and peaks fitting were performed using Casa XPS software. All spectra are presented charge balanced and energy referenced to C 1s at 284.6 eV. Chemical states of Ag, O, N and C species were determined from the charge corrected high resolution scans.

2.2.6.7. UV Spectrophotometer

UV-Vis spectra analysis of sample and p-NP Reduction monitoring was done using Perkin Elmer Lambda 35 spectrophotometer

2.2.6.8. SERS measurements

SERS spectra were acquired using a Micro Raman model STR 500, equipped with an Nd-YAG laser at 532 nm, a Peltier-cooled CCD detector (-70°C) coupled to a Nichrome microscope. Calibration was carried out daily by recording the Raman spectrum of an external naphthalene standard. A spectral range of $80\text{-}2460\text{cm}^{-1}$ was obtained using the diffraction grating of 600 lines/mm. The spectra were recorded with the accumulation of two scans at a rate of 30s scan time/second. The final SERS measurements were done using a 20X EWLD working distance microscope lens and a laser power of 5 mW.

2.2.6.9. Computation Methods of Study of Ag@Ch as SERS sensors

To investigate the underlying mechanism of surface enhancement spectroscopy of p-NP, MB and CV molecules due to the presence of Ag and chitosan, the Raman active frequencies were calculated using density functional theory implemented in Gaussian09 package (Schatz, 2013). The LanL2DZ basis set was used for calculations of model molecules (p-Np, MB and CV) with

or without Ag and chitosan. The optimized structure of p-NP, MB have Cs symmetry while CV has D₃ symmetry. The chemical enhancement factor for Raman activity of the considered systems was calculated using the expression (Sharma et al., 2020).

$$EF = (I_{SERS}/C_{SERS}) / (I_{Raman}/C_{Raman}) \quad (1)$$

Where I_{SERS} denotes intensity of Raman signal after interaction with Ag nano particles, chitosan or Ag@Ch for a particular concentration of analyte involved in SERS (C_{SERS}). I_{Raman} denotes intensity of Raman signal (without interaction with Ag nano particles, Chitosan or Ag@Ch) for a particular concentration of analyte involved in Raman (C_{Raman}). The adsorption energy of molecules with Ag, chitosan and Ag@Ch was calculated using the following expression:

$$E_{ads} = E_{molecule-x} - (E_x + E_{molecule}) \quad (2)$$

(Molecule = p-NP, MB and CV; x = Ag/chitosan/Ag@chitosan)

Where $E_{molecule-x}$ is total energy of molecule interacting with Ag nano particles /chitosan/Ag@Ch, E_x is energy of Ag nano particle or chitosan or Ag@Ch and $E_{molecule}$ is energy of p-NP, MB or CV molecule.

2.3. Result and Discussion

2.3.1. UV-Vis spectra

To ensure the formation of silver nanoparticles in Ag@Ch, UV-Vis spectra (Figure 2.1A) of the aqueous suspension of Ag@Ch were taken. A broad band from 360 nm to 460 nm with maximum absorption at 415 nm in the spectrum was observed which can be attributed to the excitation of surface plasmon vibrations of Ag atoms (Kaur et al., 2021). Chitosan can interact with silver ions through amino and hydroxyl groups present in the β -1,4-glucosamine units of the polymer.

2.3.2. IR Spectra

The infrared spectra of Ag@Ch and chitosan are shown in figure 2.1B. FTIR spectrum of pristine chitosan exhibited characteristic bands of chitosan including a broad band at 3415 cm⁻¹ (N-H and O-H stretching), 1655 cm⁻¹ (NH₂ bending) and 1030 cm⁻¹ (C-O-C stretching). A broader peak at 3415 cm⁻¹ was attributed to the deprotonated amino groups that provide binding sites to the metal analyte (Nate et al., 2018). The bands between 2880 cm⁻¹ and 2900 cm⁻¹ corresponded to alkane C-H-stretching while the bands at 1561 and 1655 cm⁻¹ were attributed

to amide II and amide I groups of chitosan respectively. The stretching vibration peaks of C–N were observed at 1030 and 1075 cm^{-1} .

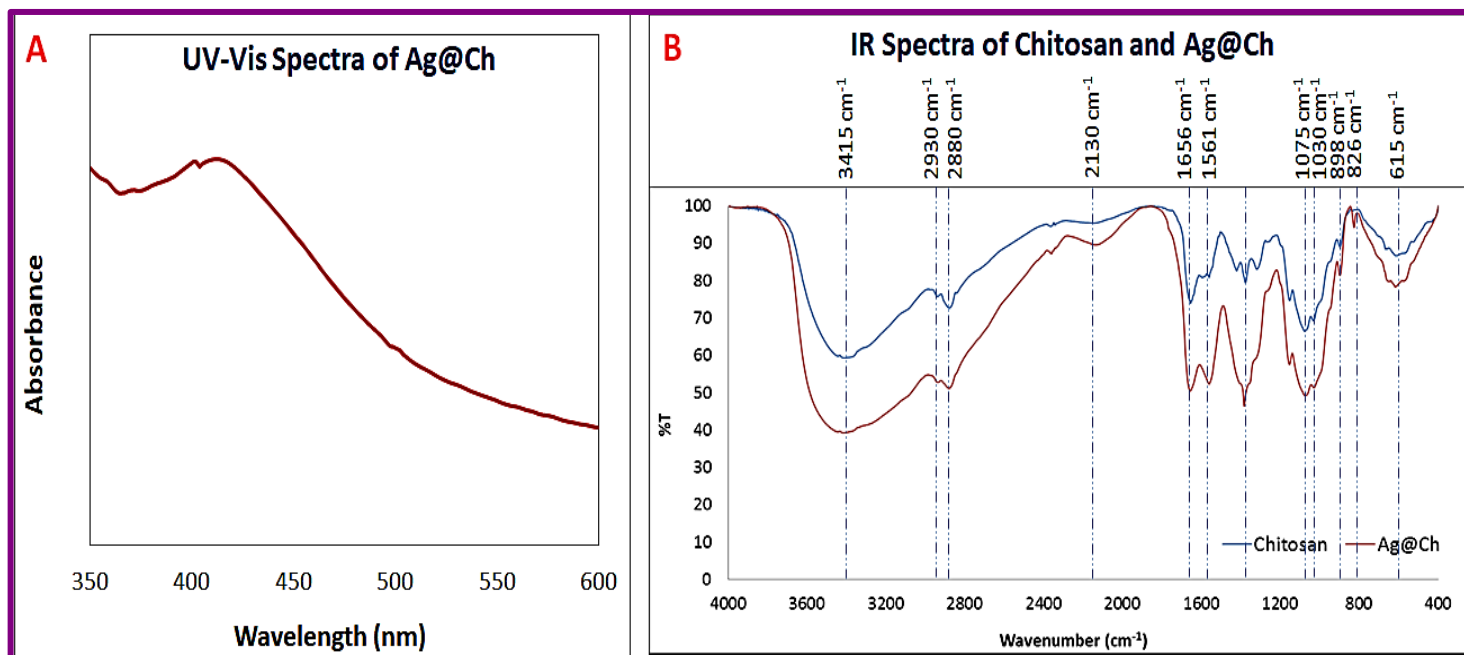


Figure 2.1: (A) UV-Vis spectra of Ag@Ch, (B) Overlay IR spectra of Chitosan and Ag@Ch

2.3.3. TG-DTA Analysis

The thermogravimetric analysis curves (TGA) and differential thermogravimetric (DTG) curves of Ag@Ch are shown in (Figure 2.2 (A&B)).

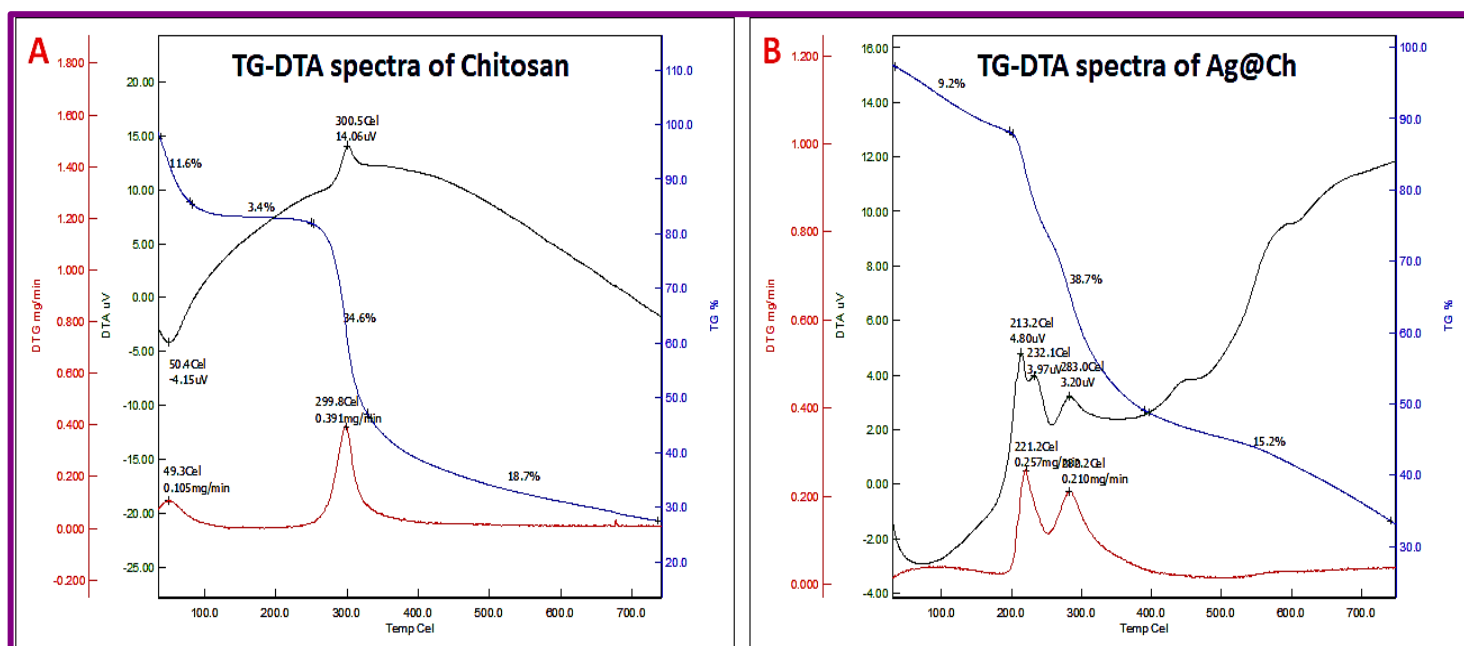


Figure 2.2: (A) TG TG-DTA curves of Chitosan and (B) TG-DTA curves of Ag@Ch

The TGA curve exhibited 3 stages of weight loss wherein the first weight loss occurred in the range of 10–200 °C corresponding to the vaporization of moisture. The second weight loss, in the range 200–400 °C may be attributed to the decomposition of acetylated and deacetylated units of chitosan as well as amine and $-\text{CH}_2\text{OH}$ group while the third weight loss at 400–700 °C can be attributed to degradation of glucopyranose residues of chitosan (Susilowati et al., 2016). The residual mass at 700 °C was about 30–40% (Liu et al., 2017).

2.3.4. SEM-EDX Analysis

The surface morphology and composition of Ag@Ch was investigated using SEM-EDS technique (Figure 2.3 (A&B)). The Ag@Ch exhibited wrinkled structures (Figure 2.3 A).

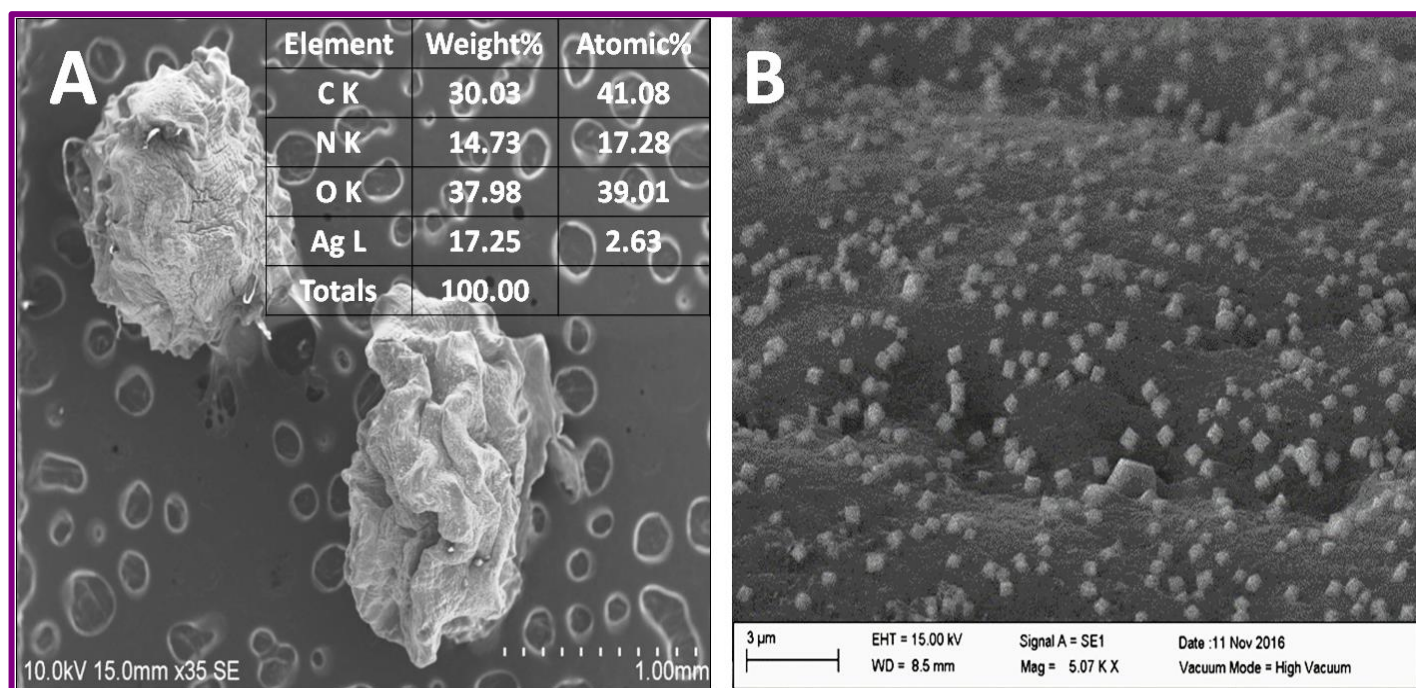


Figure 2.3: (A) SEM image of Synthesized dry Ag@Ch sample (beads), (B) SEM images silver nanoparticles homogeneously decorated on the surface of chitosan beads

SEM analysis confirmed formation of nanoparticles with near cubic shaped morphology with gaps of 0.7–1.4 nm between two nanocubes (Figure 2.3B). The EDX spectrum of Ag@Ch revealed presence of 17.25 wt% and 2.63 At% of Ag.

2.3.5. HRTEM Analysis

High Resolution transmission electron microscopy (HRTEM) images of the Ag@Ch are depicted in Figure 2.4(A-D).

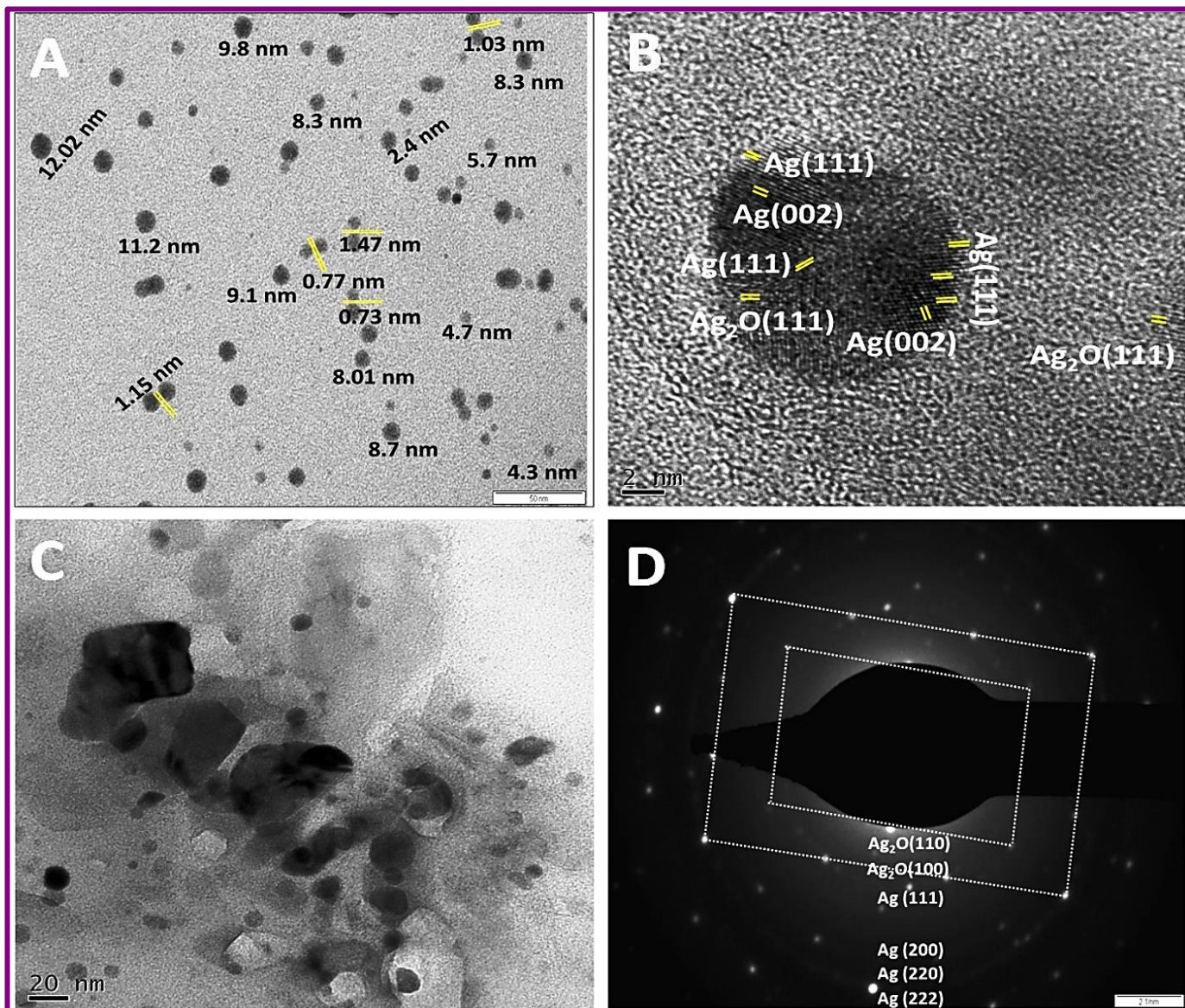


Figure 2.4: (A) TEM image of Ag@Ch, (B, C) HRTEM image of Ag@Ch, (D) SAED pattern of Ag@Ch

TEM image (Figure 2.4A) indicated that the size of well dispersed Ag NPs grown on chitosan support ranged from 3-12 nm. It was observed from HRTEM images that the cubes assembled to form rhombus shaped nanostructures on chitosan support (Figure 2.4C). Regular fringes were observed in Ag@Ch (Figure 2.4B) with spacing 0.236 and 0.21 nm indicating (111) and (002) planes of Ag(0) while the fringe with spacing 0.27 nm indicated (111) plane of Ag₂O. (M. Y. Li et al., 2016) The SAED pattern (Figure 2.4D) with bright spots indicated the *crystalline* nature of the material. The lattice plane spacings (*d*-spacings) calculated from the SAED pattern, confirmed the formation of face-centered cubic (FCC) lattice of Ag(0) & Ag₂O. (B. Li et al., 2014).

2.3.6. PXRD Analysis

Powder XRD of Ag@Ch (Figure 2.5) exhibited broad peaks at 2θ values of 38° and 64° assigned to (111) and (220) crystallographic planes respectively of the fcc structure of silver nanoparticles with trace impurities of silver oxide. Distinct broad peak at $\sim 20^\circ$ and shoulder at 9.2° were characteristic of chitosan attributed to (110) and (020) planes respectively (Hai & Sugimoto, 2018; Lynn et al., 2020; Pawara et al., 2016).

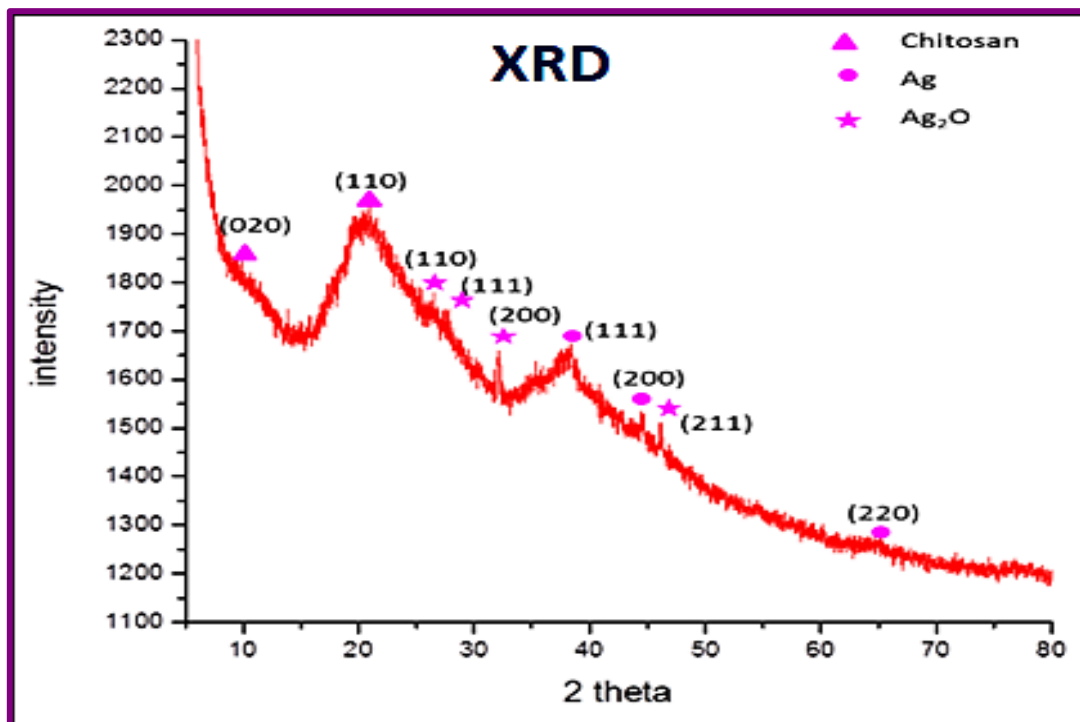


Figure 2.5: PXRD spectra of Ag@Ch

2.3.7. XPS Analysis

XPS analysis (Figure 2.6) was performed to determine the composition and oxidation states of the elements present in the synthesized nanostructure.

The XPS survey spectrum (Figure 2.6A), indicated the presence of 2.61 At% of Ag in the sample. Further, the Ag 3d core-level spectrum (Figure 2.6E) exhibited two peaks at binding energies 368.25 eV and 374.25 eV with a spin orbital coupling separation of 6 eV corresponding to 3d_{3/2} and 3d_{5/2} orbits of zero valent Ag atom. The additional Ag3d_{3/2} peak at 367.62 eV and Ag3d_{5/2} peak at 373.62 eV were attributed to Ag₂O while the peak at 369.05 eV can be attributed to metallic nano clusters smaller than 4 nm (Phukan et al., 2019).

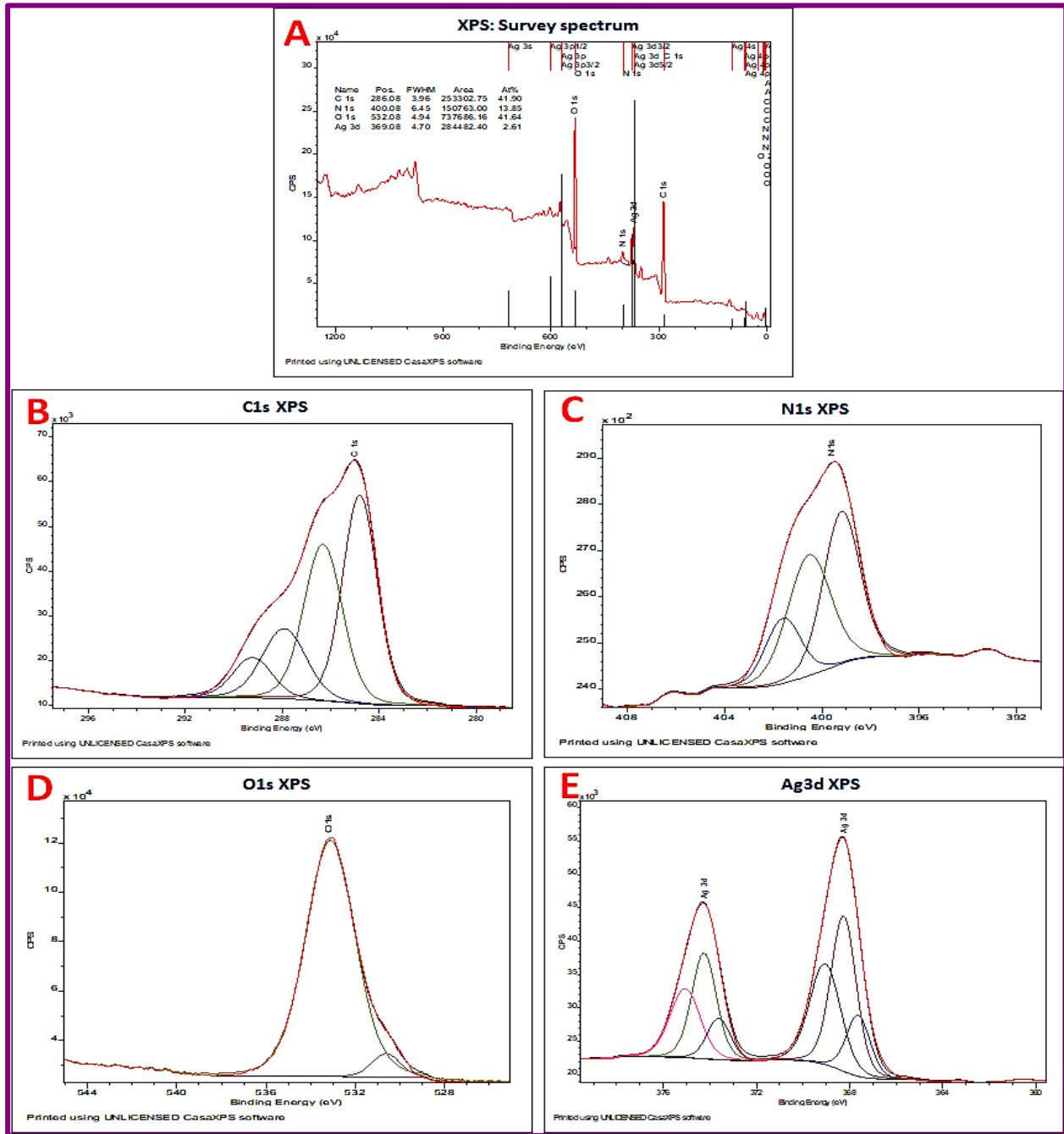


Figure 2.6:(A) Survey spectrum of Ag@Ch, (B) C 1s XPS Spectra of Ag@Ch, (C) N 1s XPS Spectra of Ag@Ch, (D) O 1s XPS Spectra of Ag@Ch, (E) Ag 3d XPS Spectra of Ag@Ch

The positive shift in binding energy relative to bulk Ag of about 1eV indicated silver nanoclusters of size smaller than 10 nm in good agreement with the HRTEM measurements. The shift to higher binding energy may be due to weaker screening of the core hole from smaller particles(Mao et al., 2014). The deconvoluted Ag3d XPS spectra confirmed that Ag is present in the form of Ag₂O (7.1 At%), Ag(0) (46.19 At%) and Ag clusters (36.7 At%).

The C 1s (Figure 2.6B) regions were fitted with four components, centered at 284.8 eV, 286.32 eV, 287.92 eV and 289.23 eV assigned to aliphatic C- C and C- H; C -N and C- O; and O- C- O bonds respectively. The N 1s XPS (Figure 2.6C) peak at binding energy of 400.53 eV was characteristic of amine group and/or amide groups while the shoulder at higher binding energy of 401.59 eV can be attributed to protonated amine groups (Carapeto et al., 2017). The XPS spectrum of oxygen (Figure 2.6D) exhibited a peak at 530.63 eV that can be assigned to C=O of *N*-acetylated glucosamine while the peak at 533.21 eV was assigned to C–O or O–H or bound water.

2.4: Applications of Ag@Ch

2.4.1. Application of Ag@Ch as SERS sensor

The effect of wet or dry acquisition conditions on the SERS enhancement has been less studied and we therefore examined the SERS by three methods as described in section 2.2.3. The acquisition of SERS while analyte was still wet (method 1) resulted in sharp characteristic peaks of the analyte. Therefore, further optimizations were done using method 1. Analyte amount was optimized with 30 ppm MB as a probe molecule (Figure 2.7). SERS signals with 10 mg substrate and 0.05 mL of 30 ppm MB solution gave the highest intensity.

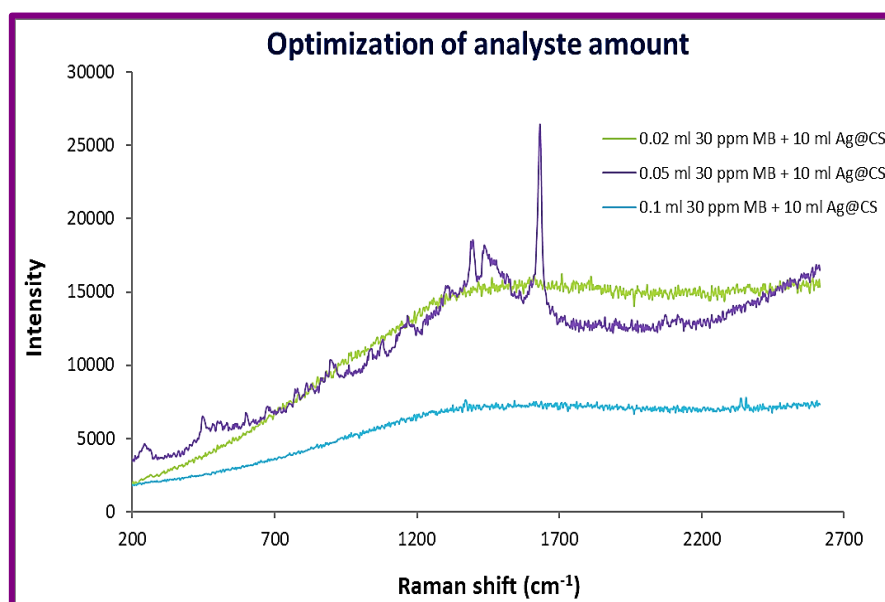


Figure 2.7: Optimization of analyte amount

After optimization of analyte amount (Figure 2.7), optimization of amount of substrate was performed with (30 ppm 0.05 mL MB) (Figure 2.8). It was observed that the highest intensity

of Raman signals was obtained with 1 mg of substrate and 0.05 mL of 30ppm analyte. Concentration study was done by using 0.05 mL of analyte and 1 mg substrate.

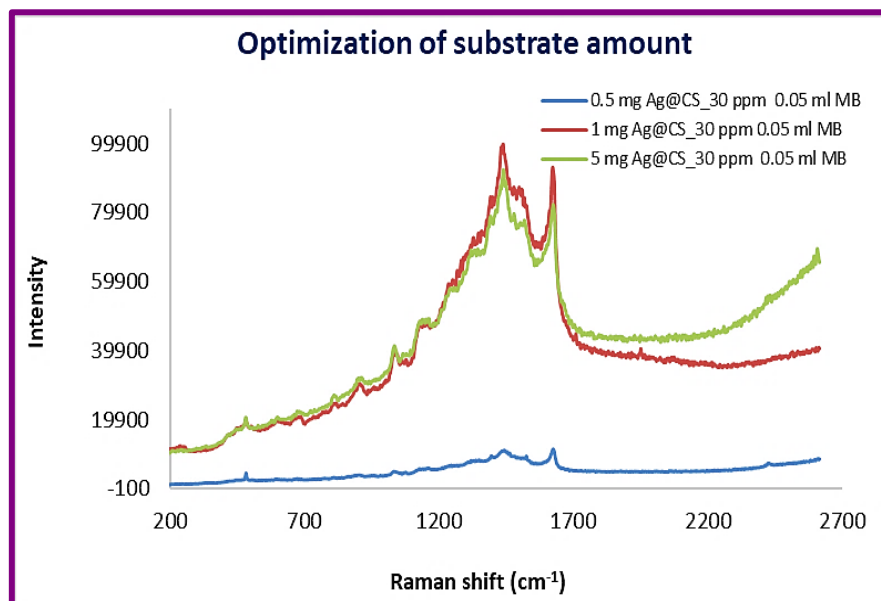


Figure 2.8: Optimization of Substrate amount

The intensity of characteristic peaks of the three analytes increased as their concentration increased (Figure 2.10) and the detailed assignments for MB, CV and p-NP are mentioned in table 2.1.

Assignment of selected SERS peaks

(A) MB (Srichan et al., 2016)		(B) CV (Meng et al., 2013)	
SERS (cm ⁻¹)	Vibrational assignment	SERS (cm ⁻¹)	Vibrational assignment
1164	C-N stretching	473	C-N bending
1394	C-H in plane ring deformation	815, 1173	C-H bending
1438	C-N asymmetric stretching	916	Ring skeletal vibrations
1525	C-C asymmetric stretching	1356	$\nu_{as}(CC_{centre}C)/\delta(CCC)_{ring}/\delta(CH)$
1624	C-N _{ring} , C-C stretching	1593, 1627	-C-C stretching of phenyl ring

(C) Assignment of selected SERS peaks of p-NP (J. Wang et al., 2020) (Muniz-Miranda, 2014)

SERS (cm ⁻¹)	Vibrational assignment	SERS (cm ⁻¹)	Vibrational assignment
820, 953	$\delta(\text{CH})_{\text{op}}$, $\delta(\text{CH})_{\text{op}}$	1400	(CH) _{ip} bend
1250	C-O stretch	1500	(NO ₂) asymmetric stretch
1323	(NO ₂) symmetric stretch	1557	(CH) _{ring} stretch

Table 2.1: (A) Assignment of selected peaks of MB, (B) Assignment of selected peaks of CV, (C) Assignment of selected peaks of p-NP

The main UV-Vis absorption peaks of the MB solution (Figure 2.9) were located at ~663, 610 and 293 nm. It meant that all peaks were away from the excitation wavelength, thus there may be no significant resonant Raman contribution to these peaks as the laser excitation wavelength was 532 nm.

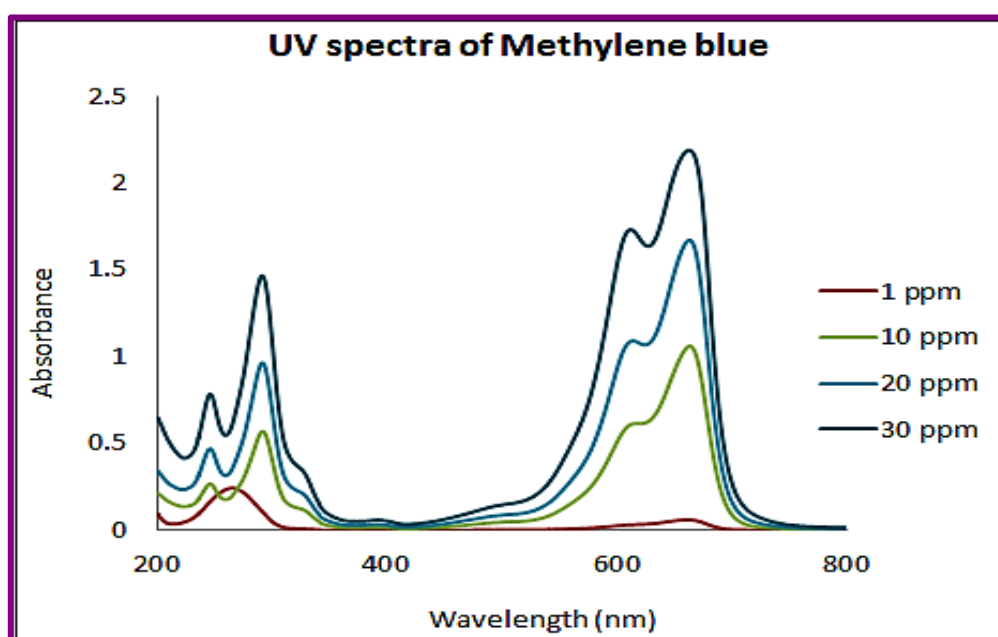


Figure 2.9 UV-Vis spectra of 1-30 ppm Methylene blue dye

Apart from the characteristic peaks of MB (Figure 2.10(A&B)), a strong band was observed at 483 cm⁻¹ for 1-10 ppm of methylene blue which can be attributed to the in-plane bending mode of thiazine group of monomeric form of methylene blue suggesting that a significant amount

of monolayer was formed on 1 mg Ag@Ch in the studied concentration range. On increasing the concentration of methylene blue to 30 ppm another signal at 456 cm^{-1} was also observed which can be attributed to dimeric form of MB (Fateixa et al., 2017). Further a peak at $\sim 246\text{ cm}^{-1}$ usually not observed in Raman spectra of methylene blue was observed which is ascribed to Ag-N stretching of the Ag-MB complex.

The SERS spectrum of CV (Figure 2.8(C&D)) exhibited peaks at 1627 and 1593 cm^{-1} , corresponding to the C-C stretching vibration of the phenyl ring. The peak at 1356 cm^{-1} was ascribed to the C-C stretching vibration, and those at 1173 and 815 cm^{-1} were ascribed to C-H bending vibrations. The ring skeletal vibration and C-N bending vibration occurred at 914 and 473 cm^{-1} , respectively. Since the excitation wavelength (532 nm) falls at 61% of CV's wavelength of absorption maximum (586 nm) (Maxwell & Tong, 2016), there is a Raman resonance effect along with the surface-enhanced Raman effect for detecting CV molecules. The interaction of adsorbed molecules with the metal surface is responsible for chemical enhancement, while localised surface plasmon resonance is responsible for electromagnetic enhancement (Guo et al., 2015).

The main characteristic peaks observed in SERS spectra of p-NP are listed in table 2.1(C). The two most prominent peaks were observed at 1320 cm^{-1} and 1250 cm^{-1} which may be attributed to NO_2 symmetric stretch and C-O stretch of nitrophenol ((Figure 2.10(E&F)). The nitrophenol may be adsorbed via nitro group (prominent peak at 1320 cm^{-1}) as well as through oxygen of hydroxyl group by electrostatic attraction (Muniz-Miranda, 2014; J. Wang et al., 2020). Shifts in the SERS peaks were observed for all the three probe molecules under study as compared to theoretical peak positions and literature reported SERS signals (Srichan et al., 2016) which can be attributed to difference in interactions. Chemical adsorption of all the analytes on SERS substrate was confirmed by the Ag-N stretching vibration at 242 cm^{-1} in MB, 253 cm^{-1} in CV, 289 cm^{-1} in p-NP SERS spectra. (Meng et al., 2015)

From concentration study of MB, CV & p-NP (Figure 2.10), the intensity of the major peaks at 1441 cm^{-1} for increasing MB concentration (0.001 to 30 mg/L), at 1180 cm^{-1} for increasing CV concentration (0.001 to 30mg/L) and at 1562 cm^{-1} for increasing p-NP concentration (0.001 to 30 mg/L) were used to establish the linearity between the respective analyte concentration and the intensity of their respective characteristic SERS peaks. As shown in Figure 2.8 a linear relationship between the analyte concentration and the intensity of characteristic peaks was obtained with coefficient of determination (R^2), 0.9982, 0.9997 and 0.9987 for MB, CV and p-

NP respectively, indicating that it is possible to quantify the analytes using Ag@Ch nanoparticles as SERS substrates.

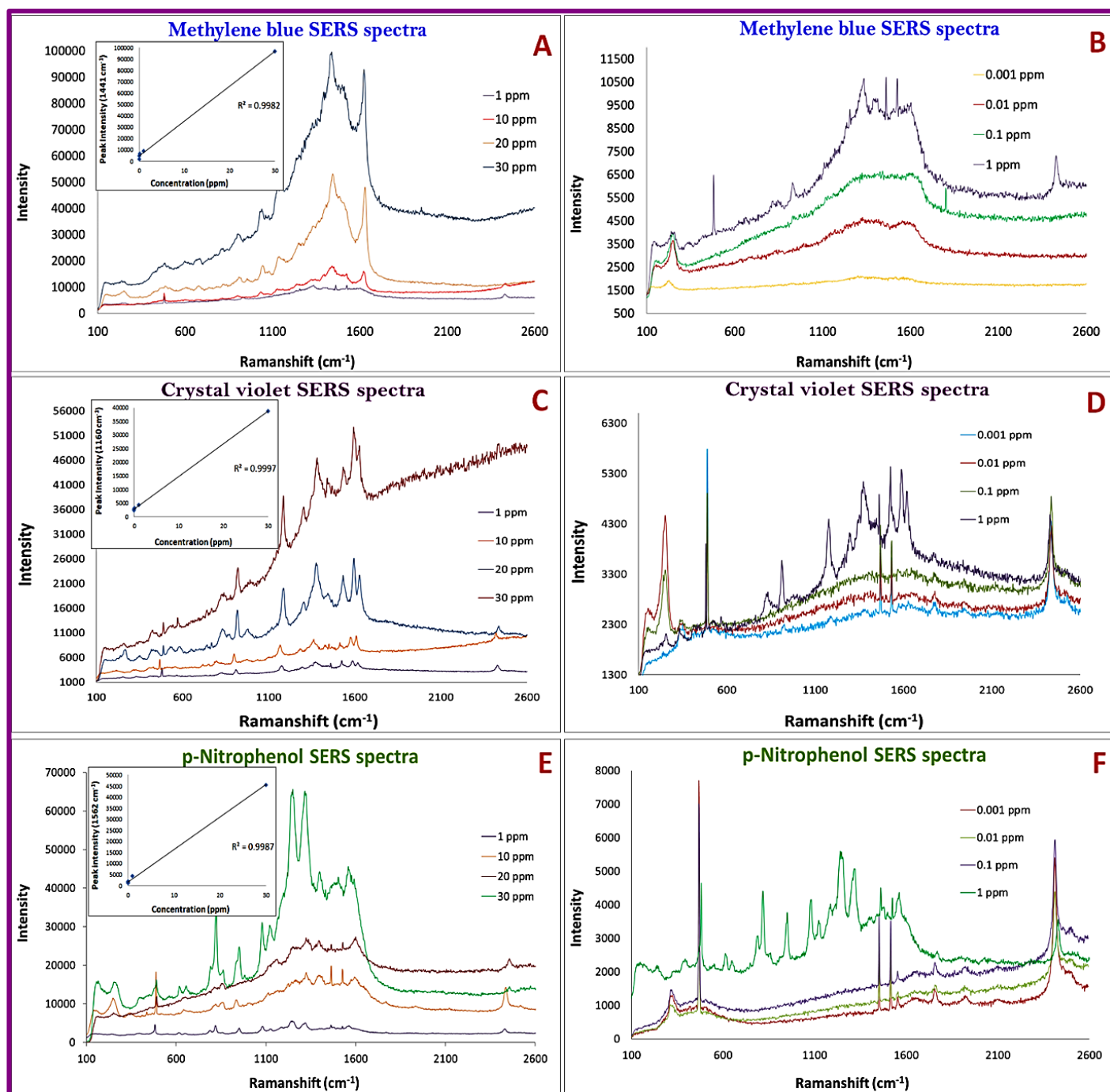


Figure 2.10 SERS measurements of (A) methylene blue, (B) Crystal violet and (C) p-Nitrophenol with chitosan supported silver nanostructure using method 1

To determine the limit of detection (LOD) and limit of quantification (LOQ) of Ag@Ch as the SERS nanoprobe, Raman spectra of aqueous samples of MB, CV and p-NP of various concentrations were collected. Using the major Raman peaks, the LOD for MB, CV and p-NP

was calculated to be 3.89 ppb, 8.13 ppb and 8.2 ppb respectively with Ag@Ch. Similarly, LOQ of Ag@Ch was determined to be 12.98 ppb, 27.09 ppb and 27.3 for MB, CV and p-NP respectively. It was thought that the larger size of CV molecule led to lower density on the metallic surfaces and may be partly responsible for its relatively lower sensitivity than that of MB(Shin et al., 2013).

Further, SERS measurements were carried out using method 2 (dried samples). Intensity of the SERS signals were increased with increase in concentration of analyte but all characteristic peaks of analytes were not observed. (Figure 2.11)

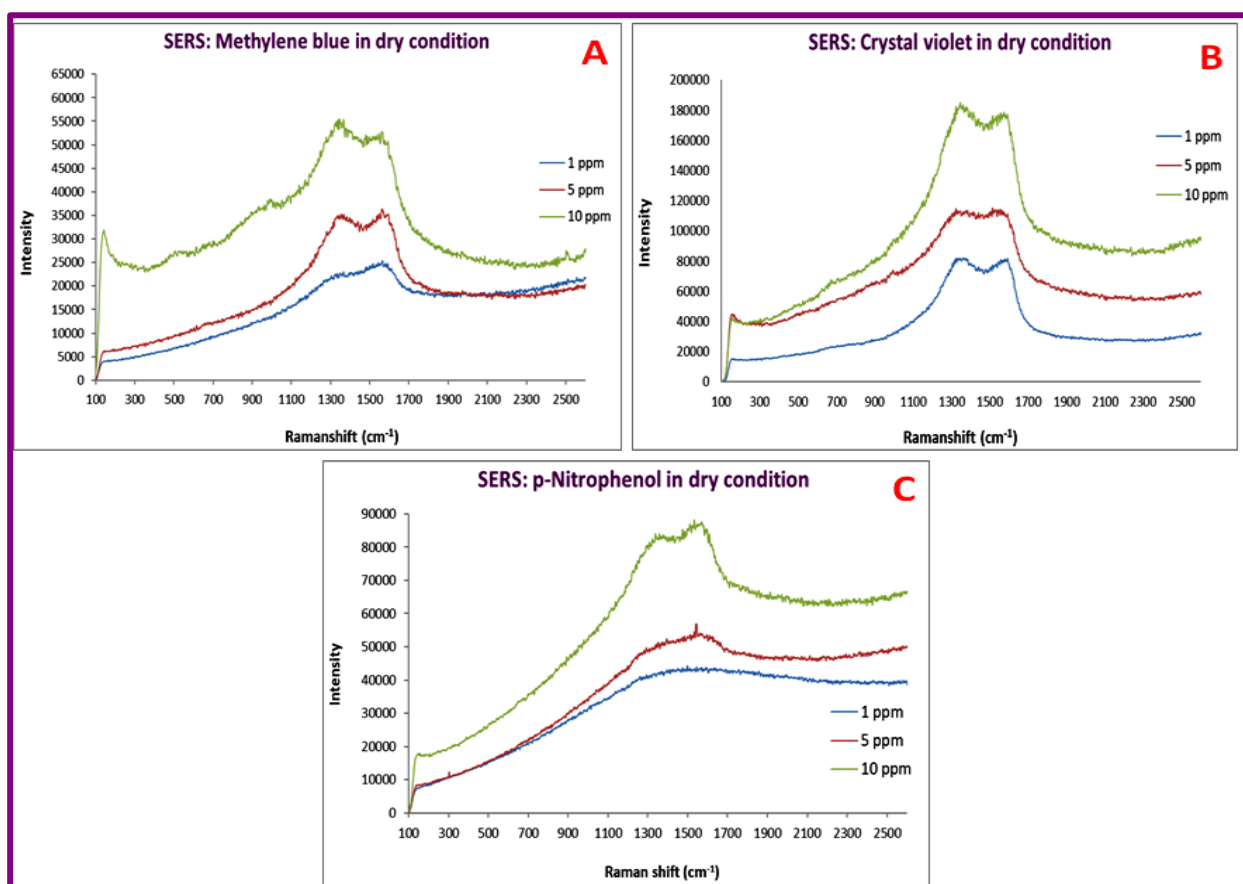


Figure 2.11: SERS measurements of (A) methylene blue, (B) Crystal violet and (C) p-Nitrophenol by using method 2

Interestingly, all spectra exhibited two prominent features due to C-C and C-O stretching/ C-H wagging/ ring breathing at $\sim 1300-1400$ cm⁻¹, C-C-C asymmetric stretching C-C ring stretching at $1500-1600$ cm⁻¹ that were seen typically enhanced with all the analytes under study. This indicated the direct interaction of benzene ring moiety with the metal surface with the analyte molecule lying flat on the metal surface(Sanchez-cortes & Ramos, 2000) and the probability of high direct ring π orbital to metal interaction (Giese & McNaughton, 2002; Son

et al., 1994) when dried. It is to be noted that these peaks were not observed in the Raman spectrum scan of chitosan/Ag@Ch/analyte separately.

The bond weakening in the benzene ring system was caused by the back donation of the metal d electrons to the benzene ring antibonding π^* orbitals (Son et al., 1994). C–H out-of plane bending vibrations at 930 cm^{-1} , 896 cm^{-1} , 842 cm^{-1} and 760 cm^{-1} are not prominent but with medium intensity in SERS spectrum. The absence of C–H stretching vibrations and the observed C–H out-of-plane bending modes suggested that the analyte molecules may be adsorbed in a flat orientation to the surface (Sajan et al., 2008).

The advantage of dried samples is that it can be transported to long distances for analysis and with high enhancement factors at very low concentrations. However, the spectra obtained were not unique to the analyte molecule and hence Ag@Ch using method 2 can function as a universal sensor.

It is important that a reading can be acquired as soon as the sample is applied to minimize waiting time (Method 3). SERS spectra with 0.05 mL of 30 ppm analyte (MB, CV, p-NP) and 1 mg Ag@Ch were acquired using method 3 (Figure 2.12). Characteristic peaks of analytes were observed and intensity of SERS peaks increased with increase in analyte concentration though the peak intensities were lower than that acquired through methods 1 and 2.

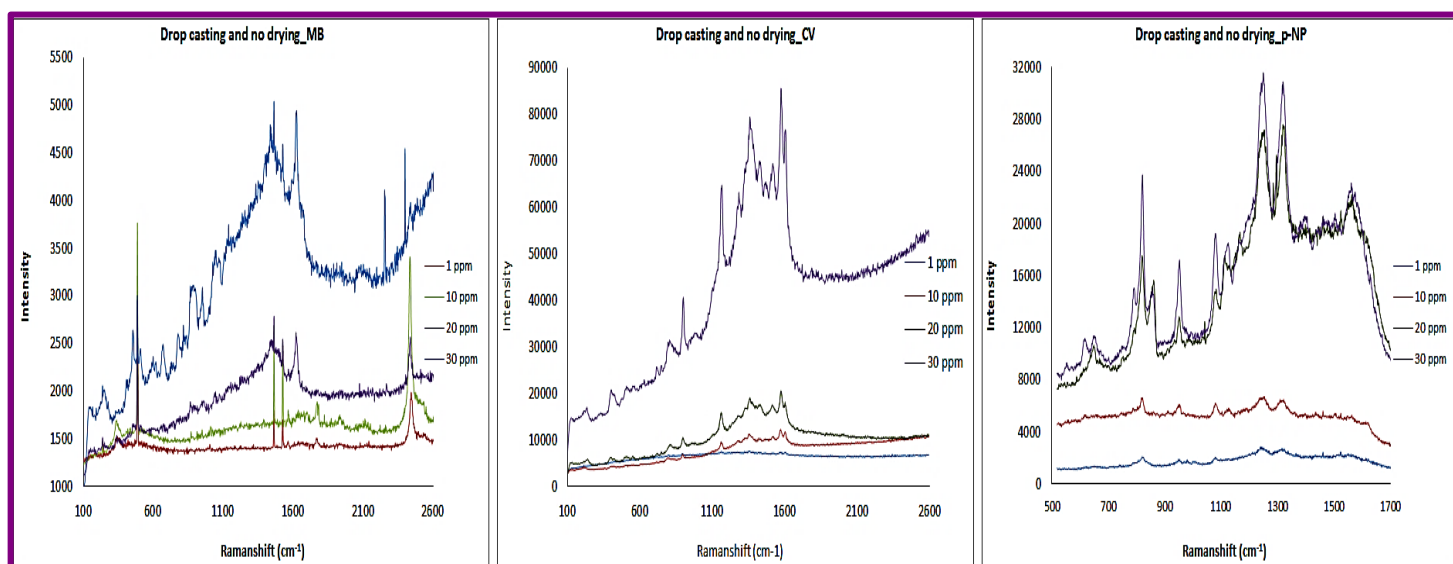


Figure 2.12: SERS measurement of liquid samples using method 3

To affirm the participation of silver in SERS phenomenon, experiments were performed in absence of silver using 1, 5, 10 mg of chitosan (Figure 2.13) only and 0.05 mL of 30 ppm

analyte under study. It was observed that the spectra did not exhibit characteristic Raman signals of the probe molecules under study. These results demonstrate that the SERS effect for the analyte molecules were because of the presence of the Ag@Ch nanostructures.

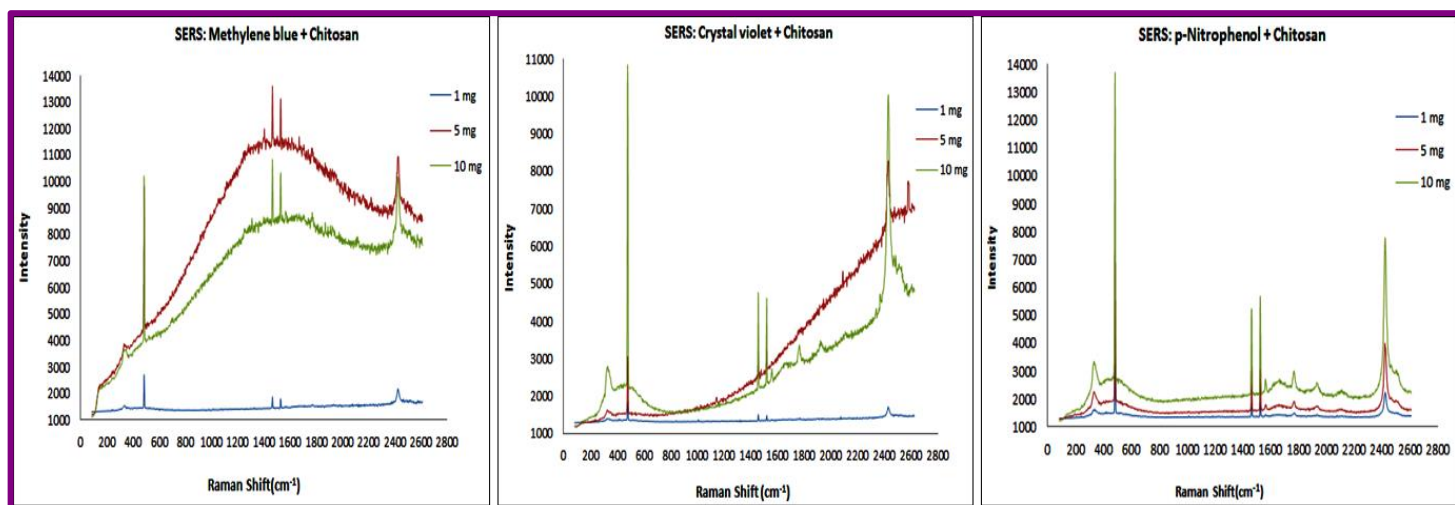


Figure 2.13: SERS measurements with Chitosan using method 1

The wrinkles in Ag@Ch provides pathways for water to permeate through, which may have helped the analyte molecules to be concentrated on the nanostructures' SERS hot spots and orient themselves amenably at the zone of the Ag NP electromagnetic field via electrostatic and π - π stacking interactions in method 1. This may have resulted in large intensification of the Raman signals of the probe molecules of interest. A similar mechanism has been proposed by Lu-Lu Qu et al(Qu et al., 2016).

The wavy structure of chitosan decorated with nanocubes of Ag present as clusters and as dimers provided the necessary hot spots for SERS enhancement.

2.4.2. Elucidation of enhancement mechanism by DFT studies

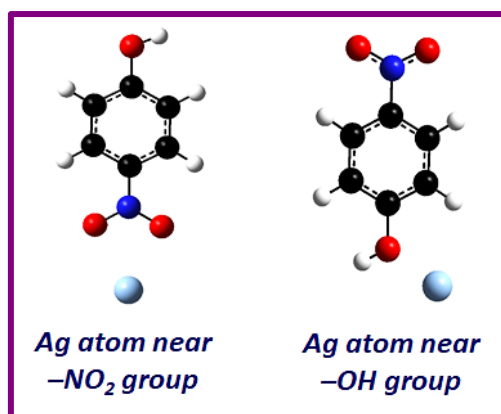
The elucidation of enhancement mechanism was attempted by considering one to four Ag nano particles interacting with analyte molecules under several conditions.

The p-nitrophenol has 3N-6 modes (15 atoms comprising 6 carbons forming benzene ring, one nitrogen, three oxygens and five hydrogen atoms), out of which 30 modes are related to benzene rings, three normal modes to OH groups and six normal modes to nitro groups. The prominently observed experimental Raman modes were compared with theoretically observed modes.

The intense peak of CO stretching vibration at 1265 cm^{-1} was observed for p-NP with LanL2DZ which was in good agreement with previous 6-311++G** basis set and comparable with experimental results(Dixit et al., 2012), while other peaks exhibited weak intensity.

Interactional Raman analysis of Single Ag atom with p-NP

The adsorption and Mulliken charge analysis of metallic Ag nanoparticle at two different positions near NO_2 & OH functional group revealed the adsorption energy to be -0.04 eV and 0.46 eV respectively.

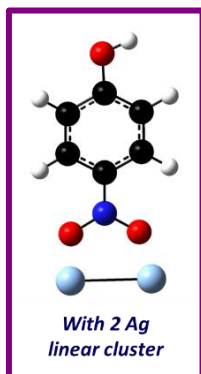


The negative sign indicated that Ag nano particle has greater binding affinity towards NO_2 as compared to OH functional group and was in energetically favourable condition. Further, charge transfer was observed between Ag and N and charge on O atoms was found to be increased. However, in case of one Ag nanoparticle towards OH group, the charge on H atom of OH functional group was found to decrease which confirmed the interaction of Ag with OH group. An enhancement of 44.52% in Raman peak attributed to asymmetric NO_2 (1521 cm^{-1}) was observed.

The decrement in HOMO and LUMO also confirmed the charge transfer mechanism between them wherein the band gap of pristine p-NP was calculated as 4.12 eV and after interaction with Ag nanoparticle it was found to be 1.6 eV . The primary contribution for SERS should thus be from chemical enhancement via CT.

Two Ag linear cluster interaction with p-NP

Further, interaction of **two Ag nanoparticle linear cluster** in the vicinity of NO_2 and OH functional groups was investigated. The most favourable configuration was towards NO_2 group with one Ag nanoparticle, and the adsorption energy increased to $\sim -1.48\text{ eV}$ as compared to one Ag nanoparticle. Enhancement was observed for the peaks 1258 and 1526 cm^{-1} that was attributed to C-O stretching and NO_2 asymmetric stretching of p-NP molecule.



Three (Triangular) and 4 Ag (linear, Rhombus) clusters interaction with p-NP

Thereafter, p-NP was interacted with triangular Ag cluster of 3 atoms, and a wire (linear) of four Ag nanoparticles as well as rhombus Ag cluster. The energy gap decreased with increase in number of Ag atoms which is independent of shape and cluster formation. It is interesting to note that the SERS enhancement was also observed for the NO₂ functional group due to charge transfer. The enhancement was observed in 1395 and 1521 cm⁻¹ modes which are of symmetric stretching and asymmetric stretching modes of NO₂ for one Ag nanoparticle while for linear **two Ag cluster**, the enhancement was observed for 1258 and 1526 cm⁻¹ as both Ag atoms are near to oxygen atoms of NO₂ function which leads to enhancement of C-O stretching and NO₂ asymmetric stretching modes of p-NP molecule.

In the triangular Ag clusters, one Ag atom remained in between two oxygen molecules of NO₂ group, which led to the suppression of the NO₂ asymmetric mode (1526 cm⁻¹). The **rhombus Ag cluster** was found to be energetically favourable compared to wire. Rhombus Ag cluster exhibited an energy gap of 1.08 eV and adsorption energy of -4.12 eV. In the case of rhombus Ag cluster, enhancement in all the peaks was observed and were in good agreement with the experimental results (Table 2.2).

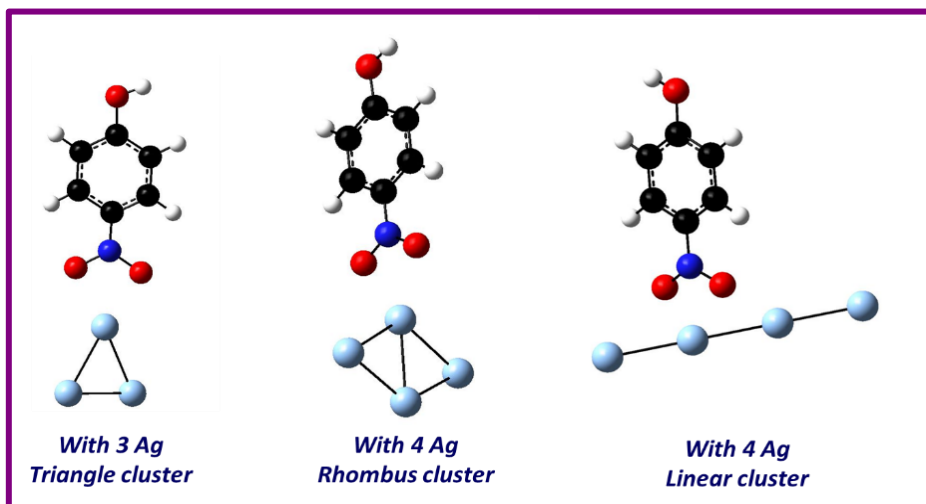


Table 2.2: Assignment of selected SERS peaks of p-NP

Assignment of selected SERS peaks of p-NP	Normal Raman mode	DFT (SERS) Ag1	Assignment of selected SERS peaks of p-NP						
			Enhancement factor (%)						
SERS	DFT(NR) cm ⁻¹	DFT (SERS) Ag1	Ag1	Ag2	Ag3	Ag4	Chitosan	1Ag@ch	4Ag@ch (P2)
820, 953	840 (826)	839	-			3.39 (838)	0.39 (841)	2.12 (841)	26.82 (854)
1250	1265, 1269 (Other DFT)	1270	-	1.2 (1258)	1.05 (1258)	4.24 (1273)	1.07 (1242)		6.39 (1269)
1323	1341 (1323)	1345	1.08		-	3.30 (1345)	1.6 (1344)	1.88 (1349)	-
1400	1423 (1423)	1395	3.65			25.95 (1411)			0.5 (1418)
1500	1529 (1528)	1521	44.52	8.76 (1526)	-	41.40 (1526)			1.8 (1520)

Investigation of role of pristine chitosan in interaction with p-NP for SERS

Thereafter, the interaction between chitosan and p-NP near to NO₂ functional group was investigated as it was energetically favourable. The adsorption energy was found to be 5.0 eV and chitosan exhibited less affinity towards p-NP as compared to Ag nano particles. Further, the distance between the O (of NO₂ group of p-NP) and H (of NH₂ of chitosan) was about 1.6 Å. This distance along with the decrement in energy gap from 4.12 eV (energy gap of pristine p-NP molecule) to 3.16 eV (after interacting with chitosan) confirmed the interaction between them. The Mulliken charge analysis confirmed the charge transfer process from chitosan to p-NP. The slight enhancement observed in intensity of bands of 841 cm⁻¹ ($\delta(\text{CH})_{\text{op}}$), 1344 cm⁻¹ (NO₂⁻ symm. stretch) and 1424 cm⁻¹ ((CH)_{ip} bend) was due to low affinity.

Role of Ag - Chitosan interaction in the SERS enhancement

Further studies were directed to investigate the binding of Ag nanoparticles with chitosan and the resultant SERS enhancement due to Ag-chitosan interaction. The adsorption energy was calculated to be 0.08 eV and -1.4 eV for one and four Ag rhombus cluster respectively. In the case of four Ag atom rhombus cluster, after optimisation, the orientation changed wherein two adjacent silver atoms were facing towards nitrogen and carbon of chitosan and its negative adsorption energy indicated strong interaction as compared to single Ag nanoparticle. Investigations were done for two possible configurations viz. with one vertex and two vertices of rhombus near the NO₂ functional group of p-NP referred to as P1 and P2 respectively.

It was observed that P2 configuration exhibited better SERS enhancement as compared to P1, energetically differing by 0.4 eV. The adsorption energy of P1 (-1.1 eV) was indeed more as compared to P2 (-0.7 eV), the enhancement factor was found to be more in case of P2 due to contribution of other silver nano particles. Enhancement was observed additionally for peak at 1269 cm⁻¹ attributed to C-O stretching of p-NP for P2 configuration as compared to P1. This peak was also observed experimentally (Figure 2.10 E) confirming that the rhombus Ag nano cluster was the possible configuration for the SERS of p-NP (all intensities were normalized for comparison (Figure 2.14A).

In both the cases, chitosan was bound with Ag cluster and two silver nano particles were found to be near to the NO₂ functional group of p-NP, the distance between them was found to be 3.15 Å and 2.72 Å for P1 and P2 respectively.

The charge transfer was observed to be different for P1 and P2. For P1 configuration (Figure 2.14A), the Mulliken charge analysis revealed that charge on Ag atom alone was 0.344 eV and the other three Ag atoms were close to each other, where the charge on the middle Ag atom forming bond with other two Ag nanoparticles was 0.167 eV, -0.027 eV (near to O of NO₂ functional group) and 0.035 eV respectively. However, in the case of P2 configuration, the charges of two Ag atoms near p-NP were found to be 0.137 eV and 0.177eV respectively, with other 2 Ag atoms having charges of 0.017 and 0.158 eV respectively. These distribution of charges on the Ag cluster, altered the energy gap of the whole system and was calculated to be 0.8 eV for P2 which is much lower than P1 (1.9 eV) resulting in higher SERS in case of P2. Enhancement was observed to be more as compared to silver nanoparticle or chitosan alone, confirming that increment in SERS was due to charge transfer from chitosan to Ag nanoparticle and further interaction with probe molecule.

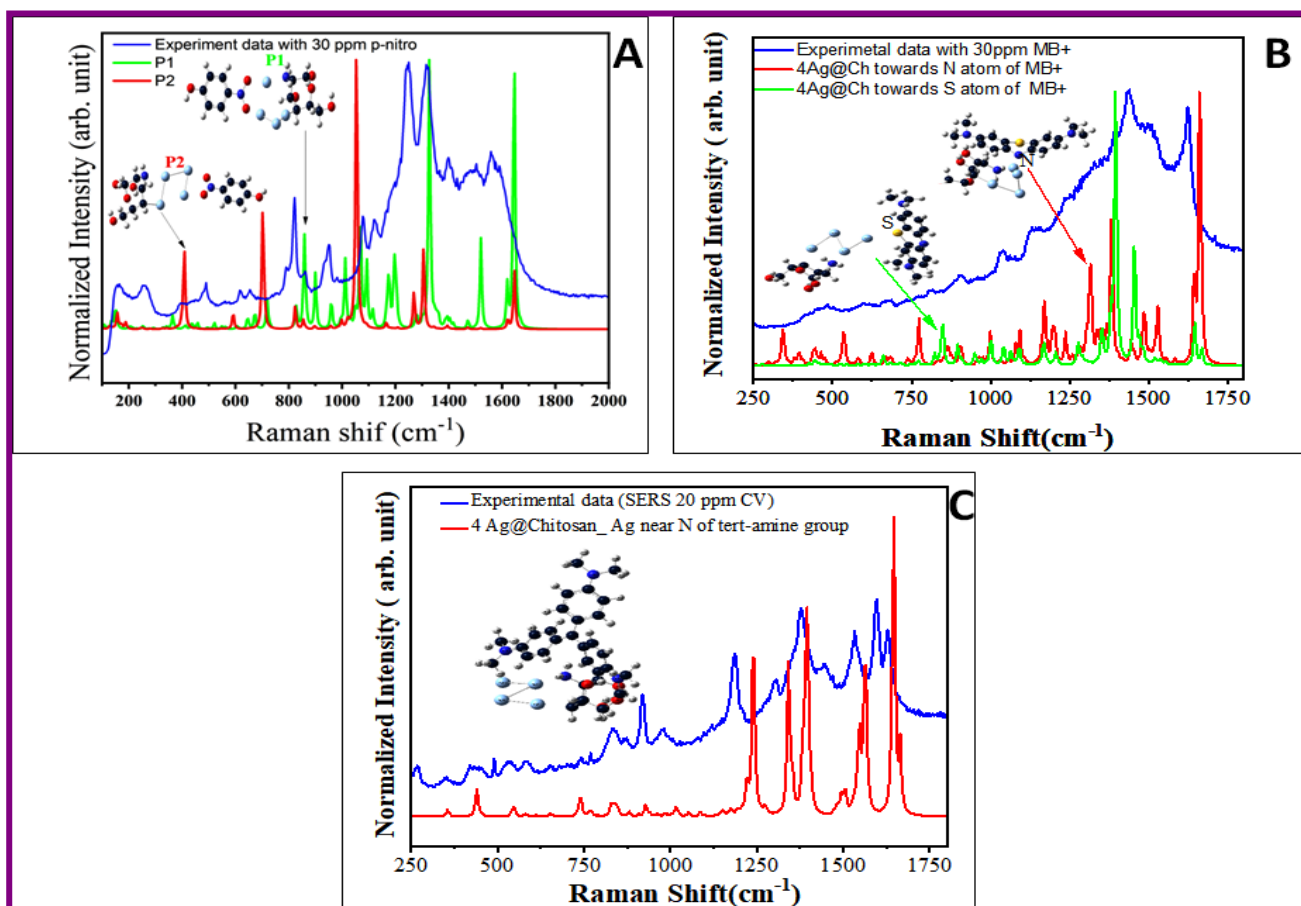


Figure 2.14: (A) Computational SERS data of p-NP, (B) Computational SERS data of MB, (C) Computational SERS data of CV

Similarly, other two molecules under study (MB and CV) were analysed and only the energetically favourable positions for conclusions were presented (Figure 2.14 B&C). Firstly, one Ag nanoparticle at two different positions was considered which was directed towards either N atom side or S atom side of thiazine group of MB at a distance of 2.2 Å in order to mimic the experimental scenario as per the previously studied protocol (Zhong et al., 2009). The nitrogen positioned configuration was found to be energetically favourable differing by -0.37 eV with adsorption energy of about -0.52 eV. After interaction with Ag nanoparticle, the charge transfer was observed from N to Ag atom, that can be validated from the energy gap decrease from -1.88 eV to -0.70 eV. A decrease in the intensity of 448.26 and 1028.46 cm^{-1} Raman peaks was observed due to bond formation between the Ag nanoparticle and MB^+ molecule (2.16 Å) which is near about 2.22 Å as observed in previous work (Zhong et al., 2009). On interaction of MB^+ molecule with chitosan, SERS was observed with 1406 and 1672 cm^{-1} Raman peaks with an enhancement factor of about 28.63% and 2.26% respectively which confirmed that chitosan played a significant role for SERS of MB^+ molecule. The interaction

of the one Ag atom with chitosan (1Ag@Ch complex) towards the N and S atom side of the thiazine group of MB⁺ molecule was investigated. It was observed that 1Ag@Ch near the N side was energetically more favourable as compared to S atom of MB⁺ molecule. The charge transfer occurred from N atom to Ag atom, being 21% lesser as compared to the single Ag nanoparticle with an energy band gap of about 0.9 eV, this alteration may be attributed to the strong interaction between the Ag nanoparticle and chitosan. The SERS enhancement was observed for C-H in-plane ring deformation and asymmetric C-N stretching and the corresponding enhancement factor was about 11% and 51% respectively. Thereafter, MB⁺ molecule was interacted with 4Ag@Ch (4 Ag atoms with Chitosan) and strong adsorption was observed. However, after optimization, 4-Ag rhombus cluster deformation and bending were observed, where two atoms were found to be on the top of N and S atom of thiazine moiety of MB⁺ molecule. The bond formation of Ag atom (on the top of N atom of MB⁺ molecule) with the carbon of chitosan atom was similar to that observed for 1Ag@Ch. However, in the case of S side of MB⁺ molecule, rhombus cluster remained intact, and it also formed bond with chitosan leading to enhancement in electric field wherein only one Ag atom was found to be near S atom of MB⁺ molecule. The adsorption energy and energy gap of 4Ag@Ch toward N atom of MB⁺ molecule was calculated to be -2.15 eV and 6.09 eV respectively. Consideration of 4Ag@Ch near N of MB⁺ (N-MB⁺) was found to be more energetically favourable with a difference of 0.9 eV from 4Ag@Ch near S. The enhancement factors for all major peaks of MB⁺ viz. 1170 cm⁻¹, 1382 cm⁻¹, 1519 cm⁻¹, 1661 cm⁻¹ were found to be 17%, 26%, 3% and 1.6% respectively. These results of SERS of MB⁺ molecules confirmed the interaction of chitosan and Ag nanoparticles indeed enhances both chemical and electric field and the optimum system is 4Ag@Ch.

Studies with MB and p-NP confirmed the binding of chitosan with Ag nanoparticles contributed to significant enhancement of the Raman spectra as compared to Ag nanoparticles alone.

The pristine eight major Raman peaks of CV⁺ molecules were at 445, 844, 927, 1174, 1356, 1544, 1578 and 1647 cm⁻¹ which were in good agreement with our experimental observations and previous theoretical investigations (Chenal et al., 2008; Gao et al., 2019). Investigation of the interaction of CV with 1Ag@Ch nanoparticles revealed an enhancement of ~ 1.0 to 1.5% for all the major peaks. The corresponding enhancement factors for 4445, 884, 928, 1175, 1356, 1544, 1578 and 1647 cm⁻¹ Raman signals were about 1.14%, 1.07%, 1.09%, 1.15%, 1.06%, 1.21%, 1.02% respectively. The enhancement was not significant as compared to p-NP

and MB⁺ molecules, due to the large size of molecules and low adsorption energy (~ -0.019 eV). However, the band gap reduced from 2.06 eV (energy gap of pristine CV molecule) to 1.32 eV (energy gap of CV molecule after interaction with 1 Ag@Ch), which can be attributed to charge transfer process taking place in between CV and Ag nanocluster. The rhombus cluster was intact, and all the four atoms were near the tert-Amine group. The interaction was strong as compared to 1Ag@Ch and adsorption energy increased from -0.019 eV to -4.41 eV with an energy gap decrease from 2.06 eV to 0.33 eV, confirming charge transfer between rhombus Ag nanocluster and CV and the predominant contribution of chemical enhancement in SERS. The highest Raman enhancement was observed due to the presence of both Ag nanoparticles and chitosan together.

Since the experiments were done in damp and liquid state (Method 1 and 3) the effect of solvation towards the Raman intensity was investigated by considering implicit water model that is Polarizable Continuum Model (PCM) (Figure 2.15). The Raman intensity of p-NP, MB⁺ and CV⁺ molecules with 4Ag@Ch was studied as the highest Raman enhancement have been observed in these systems. The adsorption energy of these molecules on 4Ag@Ch was found to be higher in solvent which is about -1.14 eV, -3.45 eV and -0.85 eV for p-NP P2 configuration, N-MB⁺ (Ag atom near N atom of Thiazine moiety) and CV⁺ molecules respectively. The observed enhancement in the Raman mode was attributed to the enhancement in charge transfer process between Ag@Ch and the probe molecules under study.

The SERS spectra in comparison with the respective pristine p-NP, MB⁺ and CV molecules were investigated. The SERS of p-NP for 842 cm⁻¹, 1272, 1325, 1400 and 1529 cm⁻¹ Raman modes was found to be enhanced by 12%, 0.41%, 0.56%, 31.91 % and 3.58 % respectively which is in good agreement with experimental findings (Figure 2.10). In the case of Methylene blue, enhancement was observed in Raman modes of C-N stretching (1192 cm⁻¹ (14 %)), C-N_{ring}, and C-C stretching (1624 cm⁻¹ (2.3 %)) while slight suppression was observed in case of C-N asymmetric stretching (1428 cm⁻¹) and C-C asymmetric stretching (1523 cm⁻¹) due to interaction between the Ag nanoparticle and thiazine group of MB⁺ molecule. However, in the case of CV molecule the highest enhancement of four-fold (459 %) for 1174 cm⁻¹ Raman mode and one-fold (112%) for 926 cm⁻¹ were observed. The enhancement in other Raman modes at 1352, 1550 and 1632 cm⁻¹ were about 2.91 %, 82% and 9.32 % respectively.

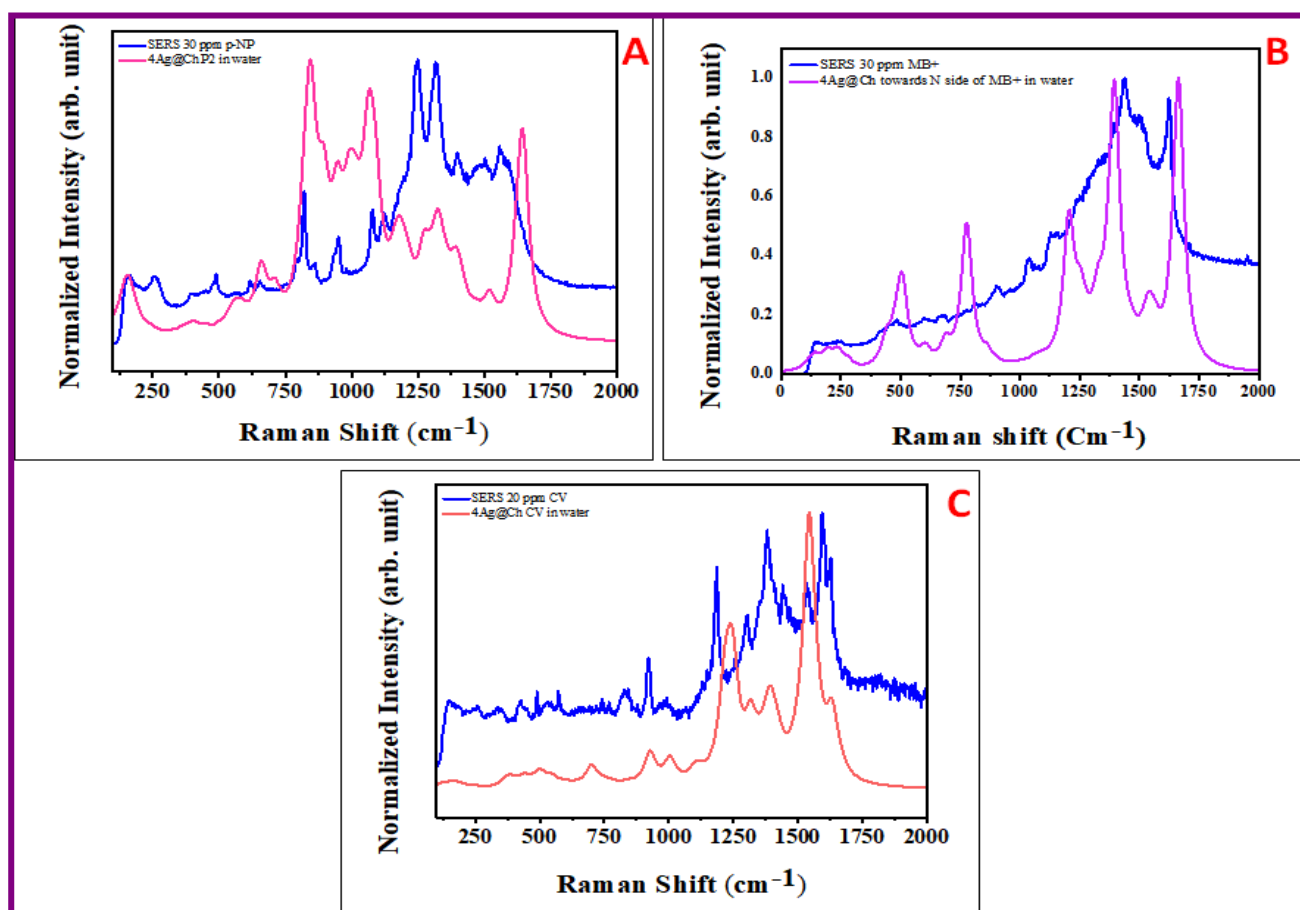


Figure 2.15: (A) Computational SERS data of p-NP, (B) Computational SERS data of MB, (C) Computational SERS data of CV with 4Ag@Ch under solvent effect

Detailed studies with MB, CV and p-NP suggested the presence of both electromagnetic and chemical enhancement with predominant chemical enhancement. Clusters of Ag nanoparticles up to 8 atoms including Ag nano chains were investigated. It was observed that chitosan can accommodate only four Ag atoms nearby and gives best results which also validated our experimental results. Only energetically favourable systems have been discussed and compared with experimental results.

2.4.3. Reduction of p-Nitro phenol (p-NP) to p-Amino phenol (p-AP)

In order to examine the catalytic activity of Ag@Ch nanoparticles, the model reaction of 4-nitrophenol (4-NP) with NaBH_4 to produce 4-aminophenol (4-AP) was used. The catalytic activity of Ag@Ch for the reduction of nitrophenol is perceived to arise due to the presence of Ag on the surface of Chitosan. In the process of reduction NaBH_4 acted as an electron donor and p-Np as an electron acceptor wherein the electrons are transferred from NaBH_4 to Ag NPs, which acts effectively as an electron relay for accomplishing the reduction. The reduction

process was monitored by UV-Vis spectroscopy (Figure 2.16) and Raman spectroscopy techniques (Figure 2.17).

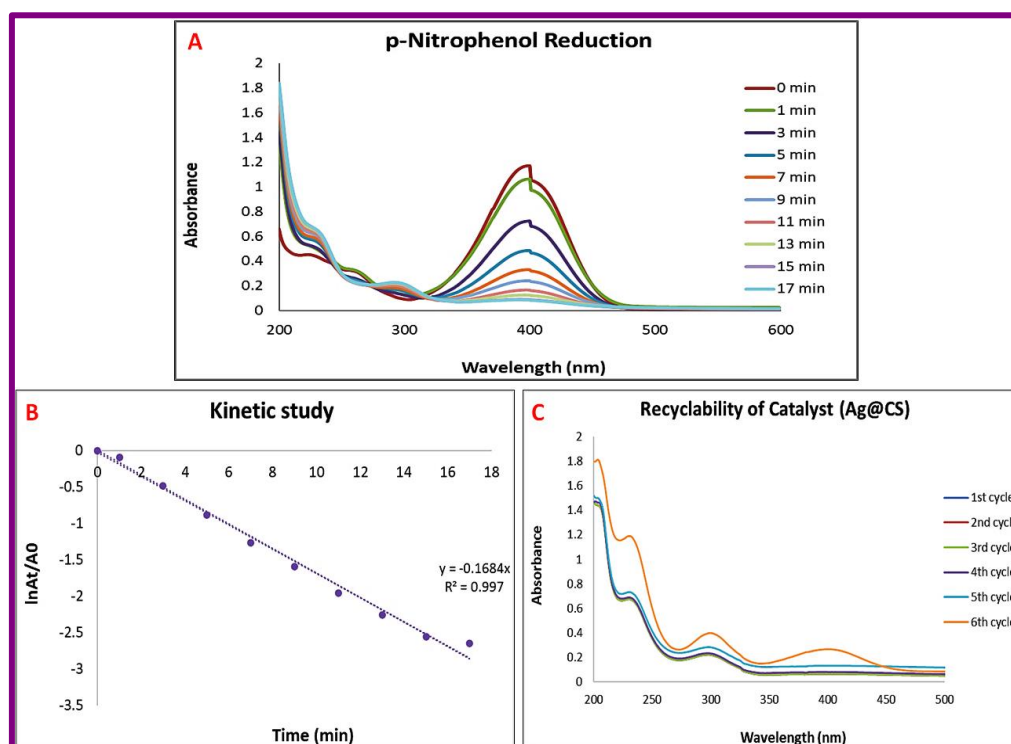


Figure 2.16: (A) *p*-Nitrophenol reduction catalysed by Ag@Ch, (B) Kinetic study of *p*-Nitrophenol reduction catalysed by Ag@Ch, (C) Recyclability study of the Ag@Ch

UV-visible absorption spectroscopy was used to monitor the reduction process of 4-NP and 4-AP, by measuring the absorption spectrum of 4-NP and 4-AP as a function of time. Figure 2.16A shows the absorption spectra of the reaction mixture at different time intervals of the reaction. With the addition of the Ag@Ch to the reaction mixture containing 4-NP and NaBH₄, a gradual decrease in the characteristic absorption peak of 4-NP at 401 nm and an evolution of a new peak for 4-aminophenol at 298 nm was observed. It is seen from the spectrum that the intensity of the absorption peak of 4-NP decreased to almost zero within 15 min. The isosbestic points at 232 nm, 298 nm and 401 nm indicated the formation of 4-aminophenol as a single product and the absence of any side reactions (Hervés et al., 2012). In control experiment, where 4-NP and NaBH₄ are used without using any catalyst, the change in intensity of the typical absorption peak of 4-NP at 401 nm was negligible indicating that 4-NP was not reduced by only NaBH₄ in 15 minutes. Further, there was no significant change in absorption band of 4-NP in the presence of only Ag@Ch. Thus, Ag@Ch nanoparticles played a significant role with NaBH₄ in the reduction of 4-NP to 4-AP.

Figure 2.16(B) shows the linear relation of $\ln(A_t/A_0)$ and reaction time (t) (where A_0 and A_t correspond to the initial absorbance of p-NP and the absorbance of p-NP at selected reaction time (t), respectively), in the p-NP reduction. This indicated that the reaction followed pseudo first order kinetics as sodium borohydride was in excess as compared to p-NP. The rate constant k , 0.1684 min^{-1} was determined from the slope proving the catalytic potential of Ag@Ch for p-NP reduction (Baran & Nasrollahzadeh, 2019).

SERS has proven particularly potent for monitoring reactions on the surface of plasmonic NPs. by analysing the evolution/disappearance or increase/decrease in intensity of SERS spectra over time (Zhou et al., 2018). Figure 2.17 shows the SERS spectra of the reaction mixture at different time intervals of the reaction. The SERS spectra of p-Nitrophenol before the start of the reaction exhibited characteristic peaks of nitrophenol as discussed in table 2.1C.

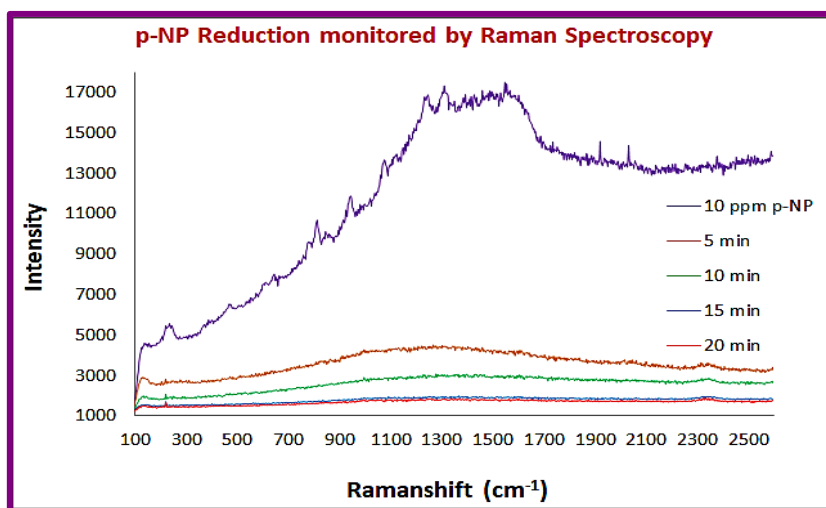


Figure 2.17: Catalytic reduction of p-Nitrophenol monitored by Raman spectroscopy

It was observed that the intensity of SERS bands of nitrophenol decreased in a span of 5 minutes and finally disappeared as the reaction progressed suggesting that the interaction of nitrophenol with Ag@Ch nanoparticles was through the nitro group. The disappearance was attributed to the lack of interaction of the aminophenol with Chitosan-Ag nanoparticles (Aditya et al., 2015). The recyclability of recovered catalysts for new rounds of reaction was examined. A complete conversion of 100% was obtained up to 5 cycles and 97.4% conversion was obtained in 6th cycle. (Figure 2.16C)

2.5. Conclusion

The complexation of Ag^+ ions with chitosan via coordinate bonding with amine and hydroxyl groups varied the reduction potential of Ag^+ and consequently changes the redox rate of AgNO_3

to Ag⁰. Due to the interaction of Ag and functional groups (–NH₂, –OH) of chitosan molecules the growth and shape were controlled by chitosan.

Chitosan biopolymer was used both as a reducing and a structure directing agent, for the crystallographic growth of Ag nanostructures. Chitosan as a capping agent aids the selective adsorption of Ag on favorable crystalline planes and induced the anisotropic growth toward that direction. The process has the advantages of one-pot and green synthesis at room temperature. The surface morphology and size of as-prepared nanoparticles was achieved by simple aging for three days

This study demonstrated for the first time that Ag@Ch can serve as universal SERS platforms if method 2 of study was adapted. This research provided new insights into surface enhanced Raman scattering associated with interaction with Ag nanoparticle, chitosan and Ag@Ch together with the effect of solvent (water). Detailed DFT studies suggested that the SERS effects are induced by the combination of chemical enhancement via charge transfer and the local EM enhancement originating from excitation of localized surface plasmons in the vicinity of the Ag nanostructures. In addition to this, the channels of chitosan generated by the wavy nature of the nanostructures further aided in enhancement of SERS signals by concentrating the analyte molecules. These unique advantages are all beneficial to improve the detection sensitivity of the fabricated SERS substrates. It was confirmed from DFT studies that chitosan can accommodate only four Ag atoms nearby and gives best results which also validated our experimental results. In case of p-NP, NO₂ functional groups exhibited higher interaction compared to OH functional group. The nitrogen atom of thiazine group was more interactive than the sulphur side of MB⁺ molecules whereas tert-amine group of CV molecules were more interactive and led to SERS. The enhancement in the particular modes of these molecules will helps in detection or sensing of these molecules.

2.6. References

- Aditya, T., Pal, A., & Pal, T. (2015). Nitroarene reduction: A trusted model reaction to test nanoparticle catalysts. *Chem. Commun.*, 51(46), 9410–9431. <https://doi.org/10.1039/c5cc01131k>
- Baran, T., & Nasrollahzadeh, M. (2019). Facile synthesis of palladium nanoparticles immobilized on magnetic biodegradable microcapsules used as effective and recyclable catalyst in Suzuki-Miyaura reaction and p -nitrophenol reduction. *Carbohydrate Polymers*, 222, 115029. <https://doi.org/10.1016/j.carbpol.2019.115029>
- Carapeto, A. P., Ferraria, A. M., & Rego, A. M. B. do. (2017). Unraveling the reaction

- mechanism of silver ions reduction by chitosan from so far neglected spectroscopic features. *Carbohydrate Polymers*, *174*, 601–609. <https://doi.org/10.1016/j.carbpol.2017.06.100>
- Chenal, C., Birke, R. L., & Lombardi, J. R. (2008). DFT , SERS , and Single-Molecule SERS of Crystal Violet Maria Vega Can. *J. Phys. Chem. C*, *112*, 20295–20300. <https://doi.org/10.1021/jp807807j> CCC:
- Chevva, H., Chandran, R., Lajeunesse, D., & Wei, J. (2017). Silver nanowires (AgNWs) growth in-situ on chitosan polymer matrix film for SERS application. *2017 IEEE 17th International Conference on Nanotechnology*, 885–889. <https://doi.org/10.1109/NANO.2017.8117319>
- Dixit, D. K., Gandhi, K., & Dixit, B. K. (2012). Theoretical calculation of hydrogen desorption energies of calcium hydride clusters. *International Journal of Hydrogen Energy*, *37*, 3767–3771. <https://doi.org/10.1016/j.ijhydene.2011.06.004>
- Duan, B., Huang, Y., Lu, A., & Zhang, L. (2018). Recent advances in chitin based materials constructed via physical methods. *Progress in Polymer Science*, *82*, 1–33. <https://doi.org/10.1016/j.progpolymsci.2018.04.001>
- Fateixa, S., Wilhelm, M., Jorge, A. M., Nogueira, H. I. S., & Trindade, T. (2017). Raman imaging studies on the adsorption of methylene blue species onto silver modified linen fibers. *Journal of Raman Spectroscopy*, *48*(6), 795–802. <https://doi.org/10.1002/jrs.5136>
- GAO, X., ZHANG, H., FAN, X., ZHANG, C., SUN, Y., LIU, C., LI, Z., JIANG, S., MAN, B., & YANG, C. (2019). Toward the highly sensitive SERS detection of bio-molecules : the formation of a 3D self-assembled structure with a uniform GO mesh between Ag nanoparticles and Au nanoparticles. *Optics Express*, *27*(18), 25091–25106. <https://doi.org/10.1364/OE.27.025091>
- Giese, B., & McNaughton, D. (2002). Surface-enhanced Raman spectroscopic study of uracil. The influence of the surface substrate, surface potential, and pH. *Journal of Physical Chemistry B*, *106*, 1461–1470. <https://doi.org/10.1021/jp011986h>
- Guo, H., Zhang, Z., Xing, B., Mukherjee, A., Musante, C., White, J. C., & He, L. (2015). Analysis of silver nanoparticles in antimicrobial products using surface-enhanced raman spectroscopy (SERS). *Environmental Science and Technology*, *49*(7), 4317–4324. <https://doi.org/10.1021/acs.est.5b00370>
- Hai, T. A. P., & Sugimoto, R. (2018). Fluorescence control of chitin and chitosan fabricated via surface functionalization using direct oxidative polymerization. *RSC Advances*, *8*, 7005–7013. <https://doi.org/10.1039/c8ra00287h>
- He, S., Chua, J., Tan, E. K. M., & Kah, J. C. Y. (2017). Optimizing the SERS enhancement of a facile gold nanostar immobilized paper-based SERS substrate. *RSC Advances*, *7*, 16264–16272. <https://doi.org/10.1039/c6ra28450g>
- Hervés, P., Pérez-Lorenzo, M., Liz-Marzán, L. M., Dzubiella, J., Lub, Y., & Ballauff, M. (2012). Catalysis by metallic nanoparticles in aqueous solution: Model reactions. *Chemical Society Reviews*, *41*, 5577–5587. <https://doi.org/10.1039/c2cs35029g>

- Jung, G. B., Kim, J. H., Burm, J. S., & Park, H. K. (2013). Fabrication of chitosan-silver nanoparticle hybrid 3D porous structure as a SERS substrate for biomedical applications. *Applied Surface Science*, 273, 179–183. <https://doi.org/10.1016/j.apsusc.2013.02.010>
- Kaur, H., Kaur, H., & Sharma, A. (2021). Materials Today : Proceedings Study of SPR peak shifting of silver nanoparticles with change in surrounding medium. *Materials Today: Proceedings*, 37(2), 3574–3576. <https://doi.org/10.1016/j.matpr.2020.09.584>
- Kumara Swamy, M., Sudipta, K. M., Jayanta, K., & Balasubramanya, S. (2015). The green synthesis, characterization, and evaluation of the biological activities of silver nanoparticles synthesized from *Leptadenia reticulata* leaf extract. *Applied Nanoscience (Switzerland)*, 5(1), 73–81. <https://doi.org/10.1007/s13204-014-0293-6>
- Li, B., Wen, X., Li, R., Wang, Z., Clem, P. G., & Fan, H. (2014). Stress-induced phase transformation and optical coupling of silver nanoparticle superlattices into mechanically stable nanowires. *Nature Communications*, 5, 4179. <https://doi.org/10.1038/ncomms5179>
- Li, M. Y., Mao, Y. Q., Yang, S. K., Dai, T. T., Yang, H., Feng, F., Wu, T., Chen, M., Xu, G. Q., & Wu, J. H. (2016). Out-of-Substrate Ag–Ag₂O Nanoplates: Surfactantless Photochemical Synthesis, Structural Evolution, and Mechanistic Study. *ACS Omega*, 1, 696–705. <https://doi.org/DOI: 10.1021/acsomega.6b00149>
- Liu, C., Wang, G., Sui, W., An, L., & Si, C. (2017). Preparation and Characterization of Chitosan by a Novel Deacetylation Approach Using Glycerol as Green Reaction Solvent. *ACS Sustainable Chemistry and Engineering*, 5(6), 4690–4698. <https://doi.org/10.1021/acssuschemeng.7b00050>
- Lynn, D., Phadke, M., & Ashok, V. D. (2020). Biogenic silver and silver oxide hybrid nanoparticles : a potential antimicrobial against. *New Journal of Chemistry*, 44, 4935–4941. <https://doi.org/10.1039/c9nj04216d>
- Maddipatla, D., Janabi, F., Narakathu, B. B., Ali, S., Turkani, V. S., Bazuin, B. J., Fleming, P. D., & Atashbar, M. Z. (2019). Development of a novel wrinkle-structure based SERS substrate for drug detection applications. *Sensing and Bio-Sensing Research*, 24(April), 100281. <https://doi.org/10.1016/j.sbsr.2019.100281>
- Mao, B., Chang, R., Shi, L., Zhuo, Q., Rani, S., Liu, X., Tyo, E. C., Vajda, S., Wang, S.-D., & Liu, Z. (2014). A near ambient pressure XPS study of subnanometer silver clusters on Al₂O₃ and TiO₂ ultrathin film supports. *Physical Chemistry Chemical Physics*, 16, 26645–26652. <https://doi.org/10.1039/C4CP02325K>
- Maxwell, E. J., & Tong, W. G. (2016). Sensitive detection of malachite green and crystal violet by nonlinear laser wave mixing and capillary electrophoresis. *Journal of Chromatography B*, 1020, 29–35. <https://doi.org/10.1016/j.jchromb.2016.02.040>
- Meng, W., Hu, F., Jiang, X., & Lu, L. (2015). Preparation of silver colloids with improved uniformity and stable surface-enhanced Raman scattering. *Nanoscale Research Letters*, 10(34). <https://doi.org/10.1186/s11671-015-0746-1>

- Meng, W., Hu, F., Zhang, L. Y., Jiang, X. H., Lu, L. De, & Wang, X. (2013). SERS and DFT study of crystal violet. *Journal of Molecular Structure*, *1035*, 326–331. <https://doi.org/10.1016/j.molstruc.2012.10.066>
- Muniz-Miranda, M. (2014). SERS monitoring of the catalytic reduction of 4-nitrophenol on Ag-doped titania nanoparticles. *Applied Catalysis B: Environmental*, *146*, 147–150. <https://doi.org/10.1016/j.apcatb.2013.03.008>
- Nate, Z., Moloto, M. J., Mubiayi, P. K., & Sibiya, P. N. (2018). Green synthesis of chitosan capped silver nanoparticles and their antimicrobial activity. *MRS Advances*, *3*(42–43), 2505–2517. <https://doi.org/10.1557/adv.2018.3>
- Nhung, T. T., & Lee, S. W. (2014). Green synthesis of asymmetrically textured silver meso-flowers (AgMFs) as highly sensitive SERS substrates. *ACS Applied Materials and Interfaces*, *6*(23), 21335–21345. <https://doi.org/10.1021/am506297n>
- Pawara, O., Deshpande, N., Dagade, S., Waghmode, S., & Joshi, P. N. (2016). Green synthesis of silver nanoparticles from purple acid phosphatase apoenzyme isolated from a new source *Limonia acidissima*. *Journal of Experimental Nanoscience*, *11*(1), 28–37. <https://doi.org/10.1080/17458080.2015.1025300>
- Phukan, S., Mahanta, A., Kakati, D., & Rashid, M. H. (2019). Green chemical synthesis of Pd nanoparticles for use as efficient catalyst in Suzuki-Miyaura cross-coupling reaction. *Applied Organometallic Chemistry*, *33*(3), 1–10. <https://doi.org/10.1002/aoc.4758>
- Potara, M., Baia, M., Farcau, C., & Astilean, S. (2012). Chitosan-coated anisotropic silver nanoparticles as a SERS substrate for single-molecule detection. *Nanotechnology*, *23*, 055501. <https://doi.org/10.1088/0957-4484/23/5/055501>
- Qu, L. L., Liu, Y. Y., Liu, M. K., Yang, G. H., Li, D. W., & Li, H. T. (2016). Highly Reproducible Ag NPs/CNT-Intercalated GO Membranes for Enrichment and SERS Detection of Antibiotics. *ACS Applied Materials and Interfaces*, *8*(41), 28180–28186. <https://doi.org/10.1021/acsami.6b08790>
- Saito, Y., Wang, J. J., Smith, D. A., & Batchelder, D. N. (2002). A Simple Chemical Method for the Preparation of Silver Surfaces for Efficient SERS. *Langmuir*, *18*(8), 2959–2961. <https://doi.org/10.1021/la011554y>
- Sajan, D., Joe, I. H., Jayakumar, V. S., & Zaleski, J. (2008). Surface enhanced Raman spectra of the organic nonlinear optic material: Methyl 3-(4-methoxy phenyl)prop-2-enoate. *Journal of Chemical Sciences*, *120*(4), 405–410. <https://doi.org/10.1007/s12039-008-0064-6>
- Sanchez-cortes, S., & Ramos, J. V. G. (2000). Adsorption and Chemical Modification of Phenols on a Silver Surface. *Journal of Colloid and Interface Science*, *231*, 98–106. <https://doi.org/10.1006/jcis.2000.7101>
- Schatz, G. (2013). The Hemiphraetid Frogs: *Cytogenet Genome Res*, *138*, 69–384. <https://doi.org/10.1159/000348293>
- Sharma, V., Som, N. N., Pillai, S. B., & Jha, P. K. (2020). Spectrochimica Acta Part A : Molecular and Biomolecular Spectroscopy Utilization of doped GQDs for ultrasensitive

- detection of catastrophic melamine : A new SERS platform. *Spectrochimica Acta Part A: Molecular and Biomolecular Spectroscopy*, 224, 117352.
<https://doi.org/10.1016/j.saa.2019.117352>
- Shin, H., Hong, J., & Huh, S. (2013). 2 - Thiopheneacetic Acid Directed Synthesis of Au Nanorosette as an SERS-Active Substrate. *ACS Appl. Mater. Interfaces*, 5(4), 1429.
<https://doi.org/10.1021/am302865b>
- Son, D. H., Ahn, S. J., Lee, Y. J., & Kim, K. (1994). Adsorption of 4-methoxybenzyl cyanide on silver and gold surfaces investigated by fourier transform infrared spectroscopy. *Journal of Physical Chemistry®*, 98(34), 8488–8493.
<https://doi.org/10.1021/j100085a031>
- Srichan, C., Ekpanyapong, M., Horprathum, M., Eiamchai, P., Nuntawong, N., Phokharatkul, D., Danvirutai, P., Bohez, E., Wisitsoraat, A., & Tuantranont, A. (2016). Highly-Sensitive Surface-Enhanced Raman Spectroscopy (SERS)-based chemical sensor using 3D graphene foam decorated with silver nanoparticles as SERS substrate. *Scientific Reports*, 6, 23733. <https://doi.org/10.1038/srep23733>
- Susilowati, E., Kartini, I., Santosa, S. J., & Triyono. (2016). Effect of glycerol on mechanical and physical properties of silver-chitosan nanocomposite films. *IOP Conf. Ser.: Mater. Sci. Eng.*, 107, 012041. <https://doi.org/10.1088/1757-899X/107/1/012041>
- Tong, Q., Wang, W., Fan, Y., & Dong, L. (2018). Recent progressive preparations and applications of the SERS substrates based on silver. *Trends in Analytical Chemistry*, 106, 246–258. <https://doi.org/10.1016/j.trac.2018.06.018>
- Wang, C., Wong, K. W., Wang, Q., Zhou, Y., Tang, C., Fan, M., Mei, J., & Lau, W. M. (2019). Silver-nanoparticles-loaded chitosan foam as a flexible SERS substrate for active collecting analytes from both solid surface and solution. *Talanta*, 191, 241–247.
<https://doi.org/10.1016/j.talanta.2018.08.067>
- Wang, J., Qiu, C., Mu, X., Pang, H., Chen, X., & Liu, D. (2020). Ultrasensitive SERS detection of rhodamine 6G and p-nitrophenol based on electrochemically roughened nano-Au film. *Talanta*, 210, 120631. <https://doi.org/10.1016/j.talanta.2019.120631>
- Wang, K., Sun, D. W., Pu, H., Wei, Q., & Huang, L. (2019). Stable, Flexible, and High-Performance SERS Chip Enabled by a Ternary Film-Packaged Plasmonic Nanoparticle Array. *ACS Applied Materials and Interfaces*, 11, 29177–29186.
<https://doi.org/10.1021/acsami.9b09746>
- Zhong, L., Hu, Y., & Xing, D. (2009). Adsorption orientation of methylene blue (MB+) on the silver colloid: SERS and DFT studies. *2009 Conference on Lasers & Electro Optics & The Pacific Rim Conference on Lasers and Electro-Optics*, 1–2.
<https://doi.org/10.1109/CLEOPR.2009.5292661>
- Zhou, L., Swearer, D. F., Robatjazi, H., Alabastri, A., Christopher, P., Carter, E. A., Nordlander, P., & Halas, N. J. (2018). Quantifying hot carrier and thermal contributions in plasmonic photocatalysis. *Science*, 362, 69–72.
<https://doi.org/10.1126/science.aaw9545>